A new class of higher-ordered/extended Boussinesq system for efficient numerical simulations by splitting operators

Stéphane Gerbi, Ralph Lteif

A NEW CLASS OF HIGHER-ORDERED/EXTENDED BOUSSINESQ SYSTEM FOR EFFICIENT NUMERICAL SIMULATIONS BY SPLITTING OPERATORS

STÉPHANE GERBI AND RALPH LTEIF

Abstract. In this work, we numerically study the higher-ordered/extended Boussinesq system describing the propagation of water-waves over flat topography. An equivalent suitable reformulation is proposed, making the model more appropriate for the numerical implementation and significantly improved in terms of linear dispersive properties in high frequency regimes due to the suitable adjustment of a dispersion correction parameter. Moreover, we show that a significant interest is behind the derivation of a new formulation of the higher-ordered/extended Boussinesq system that avoids the calculation of high order derivatives existing in the model. We show that this formulation enjoys an extended range of applicability while remaining stable. We develop a second order splitting scheme where the hyperbolic part of the system is treated with a high-order finite volume scheme and the dispersive part is treated with a finite difference approach. Numerical simulations are then performed to validate the model and the numerical methods.

Contents

1. Introduction

1.1. **The water-wave equations.** In this paper, we investigate the one-dimensional flow of the free surface of a homogeneous, immiscible fluid moving above a flat topography $z = -h_0$. The horizontal and vertical variables are denoted respectively by $x \in \mathbb{R}$ and $z \in \mathbb{R}$ and $t \geq 0$ stands for the time variable. The free surface is parametrized by the graph of the function $\zeta(t, x)$ denoting the variation with respect to its

2010 *Mathematics Subject Classification.* 35Q35, 35L45, 35L60, 76B45, 76B55, 35C07, 65L99.

Key words and phrases. Water waves, Boussinesq system, higher-order asymptotic model, splitting scheme, hybrid finite volume/finite difference scheme.

rest state $z = 0$ (see Figure 1). The fluid occupies the strictly connected ($\zeta(t,x) + h_0 > 0$) domain Ω_t at time $t \geq 0$ denoted by:

$$\Omega_t = \{(x,z) \in \mathbb{R}^2;\ -h_0 \leq z \leq \zeta(t,x)\}.$$

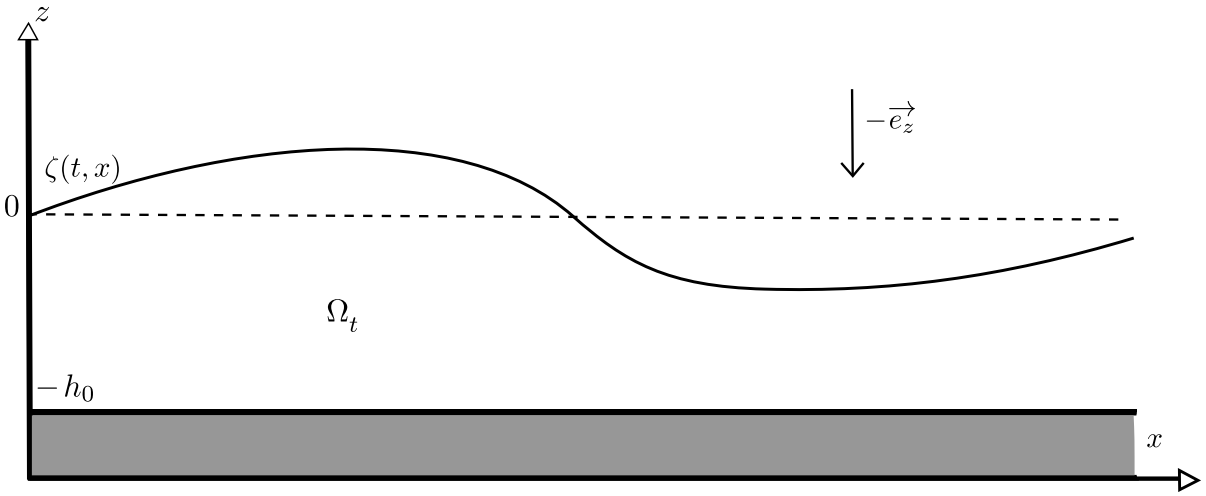

FIGURE 1. One-dimensional flat bottom fluid domain.

The fluid is considered to be perfect, that is with no viscosity and only affected by the force of gravity. We also assume the fluid to be incompressible and the flow to be irrotational so that the velocity field is divergence and curl free. We denote by (ρ, V) the constant density and velocity field of the fluid. The first boundary condition at the free surface expresses a balance of forces. Kinematic boundary conditions are considered assuming that both the surface and bottom are impenetrable, that is no particle of fluid can cross. The set of equations describing the flow is now complete and is commonly known as the *full Euler* equations:

$$\text{(1.1)} \qquad \begin{cases} \partial_t V + V \cdot \nabla_{x,z} V = -g\overrightarrow{e}_z - \nabla_{x,z} P & \text{in} \quad (x,z) \in \Omega_t,\ t \geq 0, \\ \nabla_{x,z} \cdot V = 0 & \text{in} \quad (x,z) \in \Omega_t,\ t \geq 0, \\ \nabla_{x,z} \times V = 0 & \text{in} \quad (x,z) \in \Omega_t,\ t \geq 0, \\ P|_{z=\zeta(t,x)} = 0 & \text{for} \quad t \geq 0,\ x \in \mathbb{R}, \\ \partial_t \zeta - \sqrt{1+|\partial_x \zeta|^2} n_\zeta \cdot V|_{z=\zeta(t,x)} = 0 & \text{for} \quad t \geq 0,\ x \in \mathbb{R}, \\ -V \cdot \overrightarrow{e_z} = 0 & \text{at} \quad z = -h_0,\ t \geq 0, \end{cases}$$

where $n_\zeta = \dfrac{1}{\sqrt{1+|\partial_x \zeta|^2}}(-\partial_x \zeta, 1)^T$ denotes the upward normal vector to the free surface. The theoretical study of the above system of equations is extremely difficult due to its large number of unknowns and its time-dependent moving domain Ω_t. In fact, we have a free boundary problem, in other words the domain is itself one of the unknowns.

Using the assumption of irrotational velocity field, one can express the latter as the gradient of a potential function φ. This potential satisfies the Laplace equation inside the fluid, $\Delta_{x,z}\varphi = 0$ in $(x,z) \in \Omega_t$. Consequently, the evolution of the velocity potential is written now using Bernoulli's equation. Although the system now is simpler, a free boundary problem still exists. To get over this obstacle, Craig and Sulem [11, 12] had an interesting idea following Zakharov work [45], consisting of a reformulation of the system of equations (1.1) using the introduction of a Dirichlet-Neumann operator, thus reducing the dimension of the considered space and the unknowns number. Denoting by ψ the trace of the velocity potential at the free surface, $\psi(t,x) = \varphi(t,x,\zeta(t,x)) = \varphi_{|z=\zeta}$, the Dirichlet-Neumann operator is introduced

$$\mathcal{G}[\zeta]\psi = -(\partial_x \zeta) \cdot (\partial_x \varphi)_{|_{z=\zeta}} + (\partial_z \varphi)_{|_{z=\zeta}} = \sqrt{1+|\partial_x \zeta|^2}(\partial_n \varphi)_{|_{z=\zeta}}$$

where φ is defined uniquely from (ζ,ψ) as a solution of the following Laplace problem:

$$\begin{cases} \partial_x^2\varphi+\partial_z^2\varphi=0 \quad \text{in} \quad -h_0<z<\zeta(t,x), \\ \partial_z\varphi_{|_{z=-h_0}}=0, \\ \varphi_{|_{z=\zeta}}=\psi(t,x). \end{cases}$$

with $\partial_n=n.\nabla_{x,z}$ the normal derivative in the direction of the concerned vector n. Thus, the evolution of only the two variables (ζ,ψ) located at the free surface characterize the flow. Although Zakharov's reformulation resulted in a reduced system of equations, the description of these solutions from a qualitative and quantitative point of view remains very complex. A remedy for this situation requires the construction of simplified asymptotic models whose solutions are approximate solutions of the full system. These approximate models allow to describe in a fairly precise way the behaviour of the complete system in a specific physical regime. This requires a rescaling of the system in order to reveal small dimensionless parameters which allow to perform asymptotic expansions of non-local operators (Dirichlet-Neumann), thus ignoring the terms whose influence is minimal. The order of magnitude of these parameters makes it possible to identify the considered physical regime. We start by introducing respectively the commonly known nonlinear and shallowness parameters:

$$0\leq\varepsilon=\frac{a}{h_0}=\frac{\text{amplitude of the wave}}{\text{reference depth}}\leq 1\,, \qquad 0\leq\sqrt{\mu}=\frac{h_0}{\lambda}=\frac{\text{reference depth}}{\text{wave-length of the wave}}<1\,,$$

The introduction of these dimensionless parameters allows to write the dimensionless form of the *full Euler* system:

$$\begin{cases} \partial_t\zeta-\dfrac{1}{\mu}\mathcal{G}_\mu[\varepsilon\zeta]\psi=0\,, \\ \partial_t\psi+\zeta+\dfrac{\varepsilon}{2}|\partial_x\psi|^2-\varepsilon\mu\dfrac{(\frac{1}{\mu}\mathcal{G}_\mu[\varepsilon\zeta]\psi+\partial_x(\varepsilon\zeta)\cdot\nabla\psi)^2}{2(1+\varepsilon^2\mu|\partial_x\zeta|^2)}=0\,. \end{cases} \tag{1.2}$$

where the dimensionless Dirichlet-Neumann operator $\mathcal{G}_\mu[\varepsilon\zeta]$ is now defined by:

$$\mathcal{G}_\mu[\varepsilon\zeta]\psi=-\mu\big(\partial_x\zeta\big)\cdot\big(\partial_x\varphi\big)_{|_{z=\varepsilon\zeta}}+\big(\partial_z\varphi\big)_{|_{z=\varepsilon\zeta}}=\sqrt{1+\mu\varepsilon^2\big|\partial_x\zeta\big|^2}\big(\partial_n\varphi\big)_{|_{z=\varepsilon\zeta}}$$

with φ solving the dimensionless Laplace problem

$$\begin{cases} \mu\partial_x^2\varphi+\partial_z^2\varphi=0 \quad \text{in} \quad -1<z<\varepsilon\zeta(t,x), \\ \partial_n\varphi_{|_{z=-1}}=0, \\ \varphi_{|_{z=\varepsilon\zeta}}=\psi(t,x). \end{cases}$$

The essential ingredient in constructing approximate models consists in the asymptotic expansion of the non-local operators. Replacing these operators in the *full Euler* system (1.2) by their approximations, one obtains the different asymptotic models. Many asymptotic models can be derived in the shallow water regime ($\mu\ll 1$) based on the smallness assumptions made on the nonlinear parameter ε.

1.2. **Boussinesq systems.** In what follows, we are interested in a specific long wave regime where ε is considered of the same order as μ ($\varepsilon\sim\mu$). In this regime, Boussinesq derived in [5, 6] a weakly nonlinear model bearing his name. In what follows we refer to it as the "original" or "standard" Boussinesq system. Using the horizontal depth-mean velocity

$$v(t,x):=\frac{1}{1+\varepsilon\zeta(t,x)}\int_{-1}^{\varepsilon\zeta(t,x)}\nabla\varphi(t,x,z)\,dz\,, \tag{1.3}$$

the standard Boussinesq equations reads:

$$\begin{cases} \partial_t\zeta+\partial_x\big((1+\varepsilon\zeta)v\big)=0\,, \\ \big(1-\varepsilon\dfrac{1}{3}\partial_x^2\big)\partial_t v+\partial_x\zeta+\varepsilon v\partial_x v=\mathcal{O}(\varepsilon^2)\,. \end{cases} \tag{1.4}$$

This model can be derived from the *Green-Naghdi* (GN) equations (see [20]) by neglecting all terms of order $\mathcal{O}(\varepsilon^2,\mu\varepsilon,\mu^2)$. Equivalent Boussinesq systems enjoying a better mathematical structure or physiscal propreties have been studied and derived extensively in the litterature, see for instance [1, 7, 8, 26, 29, 35, 38, 39].

To improve dispersion characteristics, shoaling and nonlinear properties, some efforts have been done to extend the Boussinesq equations to a higher order of dispersion terms, namely to include dispersive terms of order μ^2 (higher-order dispersive effects), see for instance [19, 25, 32]. Neglecting the terms

of order $\mathcal{O}(\mu^3)$ while keeping the $\mathcal{O}(\mu^2)$ terms in the equations prompt a more accurate system. The standard Boussinesq equations are restricted by containing only weak dispersion and nonlinearity. This normally limits precise applications to a small zone moderately exterior to the surf zone. Significant improvement can be made in the sense of expanding the application range and covering the range fully from deep water into the surf zone by adding higher order terms. *Extended Green-Naghdi* (eGN) equations were derived and studied in [22, 24, 33, 34]. These equations are accurate up to the order $\mathcal{O}(\mu^3)$ while the full nonlinearity is preserved. In fact, no assumption is made on the nonlinearity parameter. The extensive length of the eGN equations due to the incorporation of very high order derivatives introduce numerical complexity and have a high computational cost. In order to bring some simplifications with respect to the eGN equations, we decide to make a smallness assumption on the nonlinearity parameter, namely we consider weak nonlinearity $\varepsilon \sim \mu$. Following the work in [22, 24, 33, 34], the *extended Boussinesq* (eB) equations, can be easily obtained by dropping all terms of order $\mathcal{O}(\mu\varepsilon^2, \mu^2\varepsilon, \varepsilon^3)$. Thus, one can write the weakly nonlinear Boussinesq system including higher order dispersive effects as follows

$$\left\{ \begin{array}{l} \partial_t \zeta + \partial_x (hv) = 0 \, , \\ (1 + \varepsilon \mathcal{T}[h] + \varepsilon^2 \mathfrak{T}) \partial_t v + \partial_x \zeta + \varepsilon v \partial_x v + \varepsilon^2 \mathcal{Q} v = \mathcal{O}(\varepsilon^3) \, , \end{array} \right. \tag{1.5}$$

where $h = 1 + \varepsilon\zeta$ is the non-dimensionalised height of the fluid and denote by

$$\mathcal{T}[h]w = -\frac{1}{3h}\partial_x\big(h^3 \partial_x w\big)^{1}, \quad \mathfrak{T}w = -\frac{1}{45}\partial_x^4 w, \quad \mathcal{Q}v = -\frac{1}{3}\partial_x\big(v v_{xx} - v_x^2\big) \, .$$

This paper is devoted to the numerical study of the eB system (1.5). To this end, an equivalent (in terms of precision) suitable reformulation is proposed, making the model more appropriate for the numerical implementation.

1.3. **Outline of the paper.** In this work, we firstly propose an equivalent reformulation of the extended Boussinesq model (1.5) up to the third order, that makes the model more appropriate for the numerical implementation and significantly improved in terms of linear dispersive properties in high frequency regimes due to the suitable adjustment of a dispersion correction parameter. The reformulation is performed via two methods :

- with the factorization of high order derivatives,
- without factorization of high order derivatives.

We will show that the improvement is significant in the dispersive properties of the model with factorization of high order derivatives with an appropriate choice of optimal alpha in the high frequency regime. We then study the stability of the two models with and without factorization and we will show that factorizing only the fifth order derivative presented in the second model equation admits a destabilizing effect : we need to factor all high order derivatives.

Secondly, we propose a suitable Strang splitting of operators to solve the improved model : a hyperbolic part representing the Nonlinear Shallow Water system and a dispersive part representing the high order derivatives. The hyperbolic part of the system is treated with a high-order finite volume scheme whereas the dispersive part is treated with a finite difference method at the same order. To this end, a reconstruction of nodal unknowns and centred unknowns is presented.

Finally, numerical validations are presented, showing the interest of the extended Boussinesq model as well as the good behaviour of the numerical scheme.

1.4. **A fully justified extended Boussinesq system.** A major drawback arise in the left-most term of the second equation of (1.5) due to the positive sign in front of the elliptic fourth-order linear operator $\mathfrak{T}$ preventing the invertibility of the factorized operator, (see [23, Section 3.1]). A remedy to this situation would be replacing $(1 + \varepsilon\mathcal{T}[h] + \varepsilon^2\mathfrak{T})\partial_t v$ by $(1 + \varepsilon\mathcal{T}[h] - \varepsilon^2\mathfrak{T})(\partial_t v) + 2\varepsilon^2\mathfrak{T}(\partial_t v)$ and using a BBM trick represented in the following approximate equation $\partial_t v = -\partial_x\zeta + O(\varepsilon)$, see [22, 24] for more details. In light of these remarks and after setting $\pm\varepsilon^2\mathcal{T}[h](v v_x)$ in the second equation of (1.5), one obtains the

[1] One may realize that some components in the second order operator $\mathcal{T}$ are of size $\mathcal{O}(\varepsilon^3)$. Actually they have been kept to maintain the good properties of the operator $\mathfrak{J}$ (1.7), otherwise these properties would have been disrupt, see [23, Remark 1].

following model:

$$\begin{cases} \partial_t\zeta + \partial_x\left(hv\right) \;=\; 0, \\ \\ \mathfrak{J}\left(\partial_t v + \varepsilon v\partial_x v\right) + \partial_x\zeta + \dfrac{2}{45}\varepsilon^2\partial_x^5\zeta + +\varepsilon^2\dfrac{2}{3}\partial_x((\partial_x v)^2) = \mathcal{O}(\varepsilon^3). \end{cases} \tag{1.6}$$

where $h = 1 + \varepsilon\zeta$ and

$$\mathfrak{J} = 1 + \varepsilon\mathcal{T}[h] - \varepsilon^2\mathfrak{T}. \tag{1.7}$$

The benefit of the new formulation (1.6) is in replacing $(1 + \varepsilon\mathcal{T}[h] + \varepsilon^2\mathfrak{T})$ by a new operator $\mathfrak{J}$. This replacement induce a fifth order derivative term on ζ, namely $\dfrac{2}{45}\varepsilon^2\partial_x^5\zeta$, but the invertibility of the operator $\mathfrak{J}$ is now earned, see remark 1 in [24] for more details. An equivalent formulation of model (1.6) [2] was fully justified recently in [23]. In fact, a unique solution of the model (1.6) exist over the time scale of order $\dfrac{1}{\sqrt{\varepsilon}}$ and stay close the solution of the *full Euler* system.

Remark 1.8. Provided that the effect of surface tension is taken into consideration, the well-posedness result for system (1.6) can be directly deduced from [22, 24]. The existence time scale is up to order $1/\varepsilon$. The control of higher order derivatives resulting from the performance of the BBM trick is now possible due to the presence of surface tension which seems to be very essential (see remarks in [22]). If surface tension is neglected, which is the case in this paper, the aforementioned strategy has to be adapted. In fact, the capillary terms are replaced by a vanishing term $\pm\varepsilon^2\zeta_{xxx}$ where the negative sign term is used for a suitable definition of the energy space in such a way that the other term can be controlled. Consequently, the existence time scale reached is up to order $1/\sqrt{\varepsilon}$, see [23], which is smaller compared to the one obtained in the presence of surface tension.

2. Reformulation of the extended Boussinesq system

The system (1.6) is much easier to solve numerically than the standard formulation (1.5). In fact, the operator $\mathfrak{J}$ has an appropriate structure allowing its inversion. However, the second order dispersive operator $\mathcal{T}[h]$ present in $\mathfrak{J}$ depends on $\zeta(t,x)$ and thus on time. In fact, during the numerical computations the operator $\mathfrak{J}$ has to be inverted at each time step so one can solve equation (1.6). Following [15, 27], the time dependency has to be amended in order to reduce the computational time. Using straightforward asymptotic expansions, the left-most term of the second equation of (1.6) can be written under the form:

$$\mathfrak{J}(\partial_t v + \varepsilon v\partial_x v) = (1 + \varepsilon\mathcal{T}[0] - \varepsilon^2\mathfrak{T})(\partial_t v + \varepsilon v\partial_x v) - \frac{2}{3}\varepsilon^2\zeta\partial_x^2(\partial_t v) - \varepsilon^2\partial_x\zeta\partial_x(\partial_t v) + \mathcal{O}(\varepsilon^3),$$

where $\mathcal{T}[0]w = -\dfrac{1}{3}\partial_x^2 w$ and $\mathfrak{T}w = -\dfrac{1}{45}\partial_x^4 w$. Hence the system (1.6) is equivalent to the following model:

$$\begin{cases} \partial_t\zeta + \partial_x\big(hv\big) \;=\; 0, \\ \\ \Big(1 + \varepsilon\mathcal{T}[0] - \varepsilon^2\mathfrak{T}\Big)\Big(\partial_t v + \varepsilon v\partial_x v\Big) + \partial_x\zeta + \dfrac{2}{45}\varepsilon^2\partial_x^5\zeta + \varepsilon^2\dfrac{2}{3}\partial_x((\partial_x v)^2) \\ \quad -\dfrac{2}{3}\varepsilon^2\zeta\partial_x^2(\partial_t v) - \varepsilon^2\partial_x\zeta\partial_x(\partial_t v) = \mathcal{O}(\varepsilon^3), \end{cases} \tag{2.1}$$

where $h = 1 + \varepsilon\zeta$. The left-most factorized operator of the second equation of (2.1) is now time-independent and enjoys a structure allowing its inversion, thus can be inverted once for all numerical time steps.

2.1. A one-parameter family of extended Boussinesq equations.

The eB equations are significantly improved in terms of linear dispersive properties due to the higher-order terms existing in these equations, see [30]. Additional improvement providing a finer characterization in high frequency regimes can be brought by adjusting a dispersion correction parameter α. Following the lines in [10, 31, 44] and without affecting the accuracy of the model, we improve the frequency dispersion of problem (2.1). This is possible, if one adds to the second equation of (2.1) some terms of the same order as the equation

[2] The equivalent formulation is obtained by multiplying both sides of the second equation of system (1.6) by the water height function, h.

precision and adjusts the parameter α in an appropriate way. See section 2.3 for the discussion on the choice of the parameter α.

From the second equation of (2.1), one deduce the following approximation:

$$\partial_t v + \varepsilon v\partial_x v + \partial_x \zeta = \mathcal{O}(\varepsilon), \tag{2.2}$$

and hence, for any $\alpha \in \mathbb{R}_+^*$:

$$\partial_t v = \alpha\partial_t v - (1-\alpha)[\partial_x\zeta + \varepsilon v\partial_x v - \mathcal{O}(\varepsilon)]. \tag{2.3}$$

The second equation of (2.1) can be recast after substituting $\partial_t v$ by its approximation given in (2.3) and neglecting all terms of order $\mathcal{O}(\varepsilon^3)$

$$\Big(1+\varepsilon\mathcal{T}[0]-\varepsilon^2\mathfrak{T}\Big)\Big(\alpha\partial_t v - (1-\alpha)[\partial_x\zeta + \varepsilon v\partial_x v - \mathcal{O}(\varepsilon)] + \varepsilon v\partial_x v\Big) + \partial_x\zeta + \frac{2}{45}\varepsilon^2\partial_x^5\zeta + \varepsilon^2\frac{2}{3}\partial_x((\partial_x v)^2)$$
$$- \frac{2\varepsilon}{3}\varepsilon\zeta\partial_x^2(\partial_t v) - \varepsilon^2\partial_x\zeta\partial_x(\partial_t v) = \mathcal{O}(\varepsilon^3).$$

After straightforward computations,

$$\Big(1+\varepsilon\alpha\mathcal{T}[0]-\varepsilon^2\alpha\mathfrak{T}\Big)\Big(\partial_t v + \varepsilon v\partial_x v + \frac{\alpha-1}{\alpha}\partial_x\zeta\Big) + \frac{1}{\alpha}\partial_x\zeta + \frac{2}{45}\varepsilon^2\partial_x^5\zeta + \varepsilon^2\frac{2}{3}\partial_x((\partial_x v)^2) \tag{2.4}$$
$$- \frac{2\varepsilon}{3}\varepsilon\zeta\partial_x^2(\partial_t v) - \varepsilon^2\partial_x\zeta\partial_x(\partial_t v) = \mathcal{O}(\varepsilon^3).$$

One can also deduce from (2.2) that,

$$\partial_t v = -\partial_x\zeta + \mathcal{O}(\varepsilon). \tag{2.5}$$

Using (2.5) in the last two terms of the equation (2.4) and dropping $\mathcal{O}(\varepsilon^3)$ terms one gets:

$$\begin{cases} \partial_t\zeta + \partial_x\big(hv\big) \;=\; 0, \\ \Big(1+\varepsilon\alpha\mathcal{T}[0]-\varepsilon^2\alpha\mathfrak{T}\Big)\Big(\partial_t v + \varepsilon v\partial_x v + \dfrac{\alpha-1}{\alpha}\partial_x\zeta\Big) + \dfrac{1}{\alpha}\partial_x\zeta + \dfrac{2}{45}\varepsilon^2\partial_x^5\zeta + \varepsilon^2\dfrac{2}{3}\partial_x((\partial_x v)^2) \\ \quad +\varepsilon^2\dfrac{2}{3}\zeta\partial_x^3\zeta + \varepsilon^2\partial_x\zeta\partial_x^2\zeta = \mathcal{O}(\varepsilon^3). \end{cases} \tag{2.6}$$

Similarly, a significant improvement of the dispersive properties has been attained in the derivation of a three-parameter family of GN equations, see [9]. In here, we will limit ourselves to the one-parameter family of eB equations (2.6) for the sake of simplicity.

2.2. **Reformulation of the extended Boussinesq equations (2.6).** In what follows, we derive an equivalent model to (2.6) at the same order of precision, *i.e.* $\mathcal{O}(\varepsilon^3)$, that prevents the calculation of high order derivatives on ζ. In here, we call such a model *eB with factorized high order derivatives*. Certainly, the model enclose high order derivatives, but we make it possible not to compute them by factoring them out by $(1+\varepsilon\alpha\mathcal{T}[0])$. The price to pay is an increase in computational cost, since one needs to solve an extra linear system[3]. In fact, dropping all terms of order $\mathcal{O}(\varepsilon)$ from the second equation of (2.6), one can easily check the following:

$$(1+\varepsilon\alpha\mathcal{T}[0])(\partial_t v) = -\partial_x\zeta + \mathcal{O}(\varepsilon),$$

thus we have

$$\partial_t v = -(1+\varepsilon\alpha\mathcal{T}[0])^{-1}(\partial_x\zeta) + \mathcal{O}(\varepsilon),$$

which may be written as

$$\partial_t v = -\partial_x\zeta + \mathcal{O}(\varepsilon)\ .$$

Using the approximation $\partial_t v = -\partial_x\zeta + \mathcal{O}(\varepsilon)$, the terms $\partial_x^2\zeta$, $\partial_x^3\zeta$ and $\partial_x^5\zeta$ become respectively:

$$\partial_x^2\zeta = \partial_x\Big((1+\varepsilon\alpha\mathcal{T}[0])^{-1}(\partial_x\zeta)\Big) + \mathcal{O}(\varepsilon), \tag{2.7}$$

$$\partial_x^3\zeta = \partial_x^2\Big((1+\varepsilon\alpha\mathcal{T}[0])^{-1}(\partial_x\zeta)\Big) + \mathcal{O}(\varepsilon), \tag{2.8}$$

$$\partial_x^5\zeta = \partial_x^4\Big((1+\varepsilon\alpha\mathcal{T}[0])^{-1}(\partial_x\zeta)\Big) + \mathcal{O}(\varepsilon). \tag{2.9}$$

[3]Inverting the operator $(1+\varepsilon\alpha\mathcal{T}[0])$ requires the discretization of $(1+\varepsilon\alpha\mathcal{T}[0])A = B$ (i.e resolution of linear systems).

Replacing $\partial_x^2\zeta$, $\partial_x^3\zeta$ and $\partial_x^5\zeta$ by their expression obtained in (2.7), (2.8) and (2.9) respectively in the second equation of (2.6), one can write the eB equations with improved dispersion and factorized high order derivatives as:

(2.10)
$$\begin{cases} \partial_t\zeta + \partial_x\big(hv\big) \;=\; 0, \\ \Big(1+\varepsilon\alpha\mathcal{T}[0]-\varepsilon^2\alpha\mathfrak{T}\Big)\Big(\partial_t v+\varepsilon v\partial_x v+\dfrac{\alpha-1}{\alpha}\partial_x\zeta\Big)+\dfrac{1}{\alpha}\partial_x\zeta+\dfrac{2}{45}\varepsilon^2\partial_x^4\Big((1+\varepsilon\alpha\mathcal{T}[0])^{-1}(\partial_x\zeta)\Big) \\ \quad +\varepsilon^2\dfrac{2}{3}\partial_x((\partial_x v)^2)+\varepsilon^2\dfrac{2}{3}\zeta\partial_x^2\Big((1+\varepsilon\alpha\mathcal{T}[0])^{-1}(\partial_x\zeta)\Big)+\varepsilon^2\partial_x\zeta\partial_x\Big((1+\varepsilon\alpha\mathcal{T}[0])^{-1}(\partial_x\zeta)\Big)=\mathcal{O}(\varepsilon^3), \end{cases}$$

where $h = 1+\varepsilon\zeta$. Significant interest is behind the derivation of the eB formulation (2.10). In fact, this formulation avoid the calculation of high order derivatives which we believe will extend the range of applicability to high frequency regimes (see discussion in section 2.3), while remaining stable (see section 2.4.2).

2.3. **Choice of the parameter α.** The main comparison between any asymptotic model and the *full Euler* equations is performed at the stage of linear periodic plane wave solutions. At this point, all characteristics of the model [41] are summed up in the dispersion relation, relating the spatial wave number k and the time frequency w. It comes from the earlier linearisation of the system around some rest state. Improving the dispersive characteristics of our model require a suitable choice of the parameter α so that the dispersion characteristics of the *full Euler system* corresponds with those of the improved eB system (2.6) at the dispersion relation level. Hence, instead of choosing the α-value that reduce the error on the phase velocity for a specific value of k (limiting the improvement to monochromatic waves), we adjust this parameter so that both phase and group velocity are minimized over a range of values of $k\in[0,K]$. This can be done by minimizing a weighted averaged error introduced for this reason. Firstly, we discuss the dispersive properties of the dimensionalized version of model (2.6) and secondly we discuss the dispersive properties of the dimensionalized version of model (2.10).

First, lets go back to variables with dimensions. Setting $\varepsilon=1$ and adding the gravity term g as needed. The system of equations (2.6) reads

(2.11)
$$\begin{cases} \partial_t\zeta + \partial_x\big(hv\big) \;=\; 0, \\ \Big(1+\alpha\mathcal{T}[0]-\alpha\mathfrak{T}\Big)\Big(\partial_t v+v\partial_x v+\dfrac{\alpha-1}{\alpha}g\partial_x\zeta\Big)+\dfrac{1}{\alpha}g\partial_x\zeta+\dfrac{2}{45}g\partial_x^5\zeta+\dfrac{2}{3}\partial_x((\partial_x v)^2) \\ \quad +\dfrac{2}{3}g\zeta\partial_x^3\zeta+g\partial_x\zeta\partial_x^2\zeta=0, \end{cases}$$

where $h=h_0+\zeta$ (dimensionalized height). The dispersion relation corresponding to (2.11) can be derived by linearising first the equations about the rest state $(\tilde\zeta,\tilde v)=(0,0)$ and then looking for the corresponding plane wave solutions of the form $(\zeta,v)=(\underline{\zeta},\underline{v})e^{i(kx-wt)}$. From the first equation of (2.11) one obtains:

$$-iw\underline{\zeta}+ikh_0\underline{v}=0 \;\Rightarrow\; \underline{v}=\frac{w}{kh_0}\underline{\zeta}. \tag{2.12}$$

The second equation of (2.11) becomes:

$$\Big(1+\frac{\alpha}{3}k^2+\frac{\alpha}{45}k^4\Big)\Big(-iw\underline{v}+\frac{\alpha-1}{\alpha}igk\underline{\zeta}\Big)+\frac{1}{\alpha}igk\underline{\zeta}+\frac{2}{45}igk^5\underline{\zeta}=0. \tag{2.13}$$

Substituting $\underline{v}$ in (2.13) by its expression given in (2.12) and multiplying (2.13) by $\dfrac{-k}{i\underline{\zeta}}$ yields the dispersion relation for (2.11):

$$w^2_{\alpha,eB}=\frac{gh_0k^2\Big(1+\dfrac{(\alpha-1)}{3}k^2+\dfrac{(\alpha+1)}{45}k^4\Big)}{\Big(1+\dfrac{\alpha}{3}k^2+\dfrac{\alpha}{45}k^4\Big)}. \tag{2.14}$$

The exact dispersion relation for the dimenisonalized *full Euler* system is recalled below:

$$w^2_{F.E}=gh_0|k|\tanh(|k|). \tag{2.15}$$

For small wavenumbers, the Taylor expansions of (2.14) and (2.15) are respectively:

$$w^2_{\alpha,eB} \approx gh_0\Big(k^2 - \frac{k^4}{3} + k^6\big(\frac{1}{45} + \frac{\alpha}{9}\big) + \mathcal{O}(k^8)\Big),$$
$$w^2_{FE} \approx gh_0\Big(k^2 - \frac{k^4}{3} + \frac{2}{15}k^6 + \mathcal{O}(k^8)\Big).$$

The two previous Taylor expansions are equivalent provided that $\alpha = 1$. (See numerical test 4.4). This equivalence doest not hold any more for larger wavenumbers which makes the choice of α in (2.14) essential.

We describe hereafter a classical approach to find an optimal value of α when studying monochromatic waves of wavenumber k. Let us define firstly the linear phase and group velocities associated to (2.14) as

$$C^p_{eB}(k) = \frac{w_{\alpha,eB}(k)}{|k|} \quad \text{and} \quad C^g_{eB}(k) = \frac{dw_{\alpha,eB}(k)}{dk}.$$

After determining the value of k, we choose α such that the phase velocity $C^p_{eB}(k)$ and the reference phase velocity $C^p_S(k)$, coming from Stokes linear theory are uniform.

This strategy is only appropriate when considering a particular wavelength. However, finding an optimal value of α for a range of values of k requires the minimization the squared relative weighted error defined below:

$$\int_0^K \frac{1}{k}\Big(\frac{C^p_{eB} - C^p_S}{C^p_S} + \frac{C^g_{eB} - C^g_S}{C^g_S}\Big)^2 dk, \tag{2.16}$$

over some range $k \in [0, K]$, where $C^g_S(k)$ is the reference group velocity associated with the Stokes linear theory.

It is clearly seen that the weighted averaged error has an absolute minimum of (0.08%) in the dispersive range $0 \leq k \leq 1$. The optimum value for α is 0.8351. Nevertheless, the error starts to grow rapidly when $K \geq 2$, showing that the model (2.11) has a limited range of applicability and thus poor dispersion properties in intermediate and large wave numbers regime (see Figures 2 and 3).

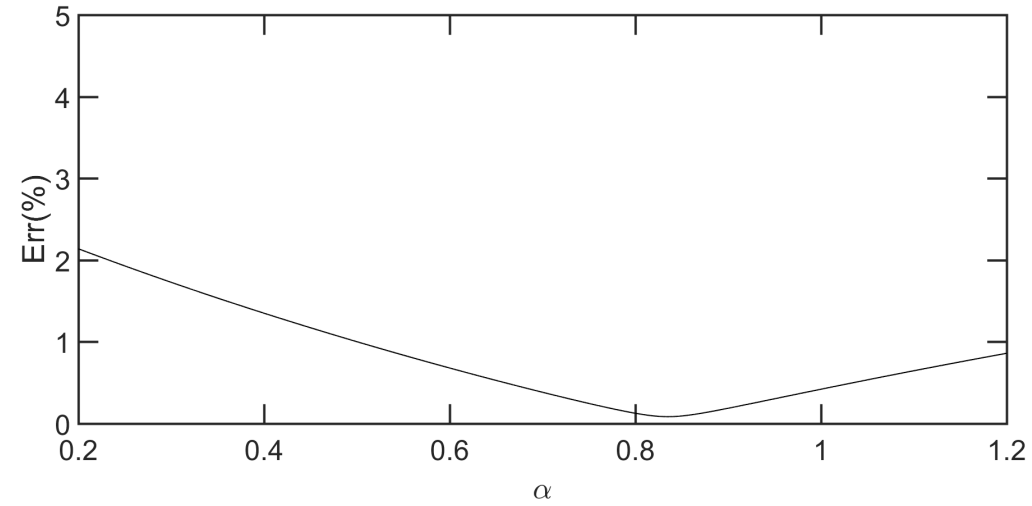

(a) $0 \leq k \leq 1$.

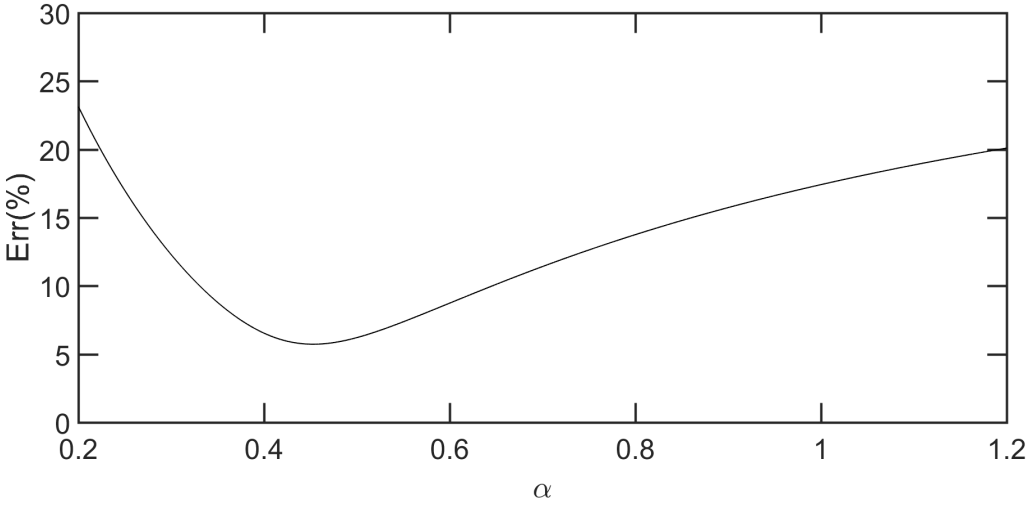

(b) $0 \leq k \leq 2$.

FIGURE 2. Phase and group velocities weighted averaged error as a function of α.

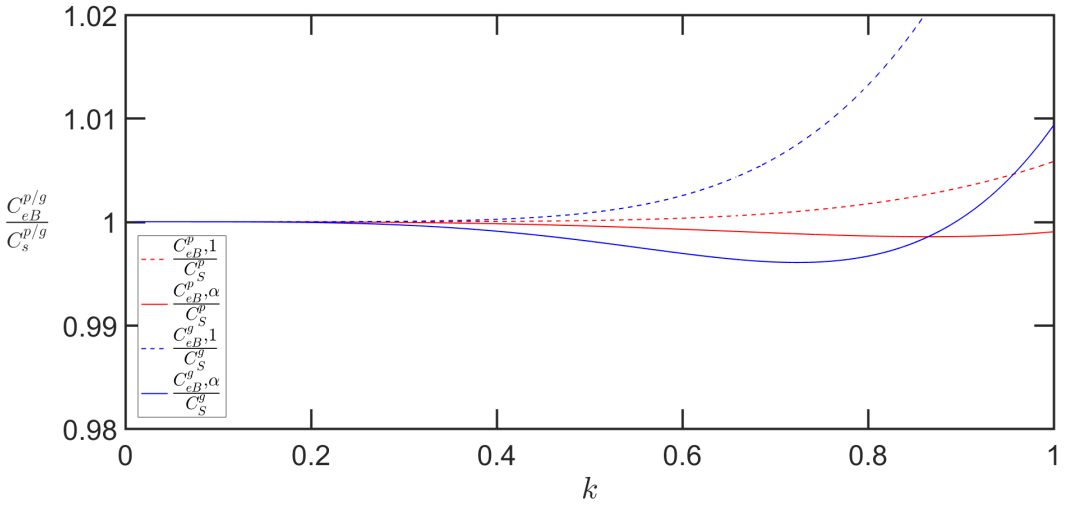

(a) $\alpha = 0.8351$ in solid lines and $\alpha = 1$ in dashes.

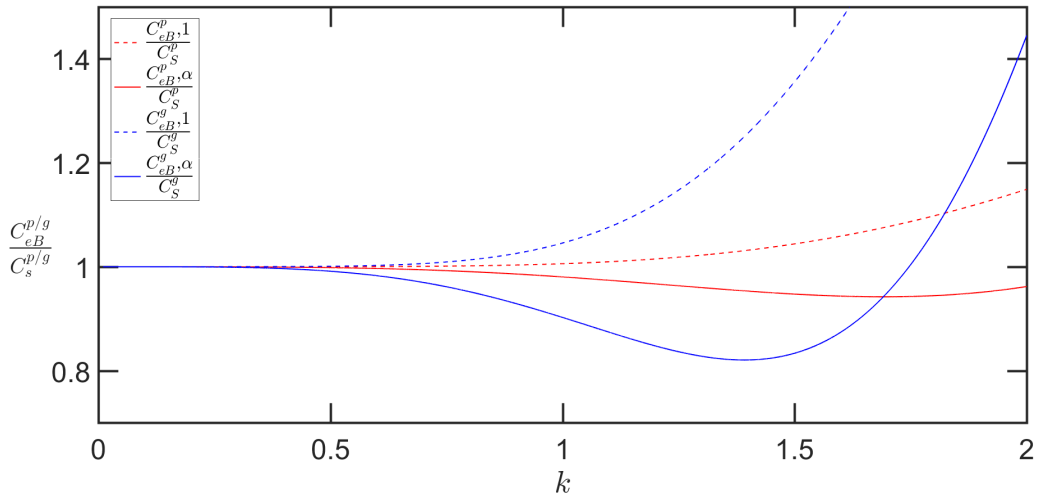

(b) $\alpha = 0.4529$ in solid lines and $\alpha = 1$ in dashes.

FIGURE 3. Errors on linear phase velocity (red) and group velocity (blue) for the eB model (2.11).

Now, we discuss the dispersive properties of the dimensionalized version of model (2.10). The dimensionalized version of equations (2.10) read:

$$
\begin{cases}
\partial_t \zeta + \partial_x \big(hv\big) \;=\; 0, \\
\Big(1 + \alpha\mathcal{T}[0] - \alpha\mathfrak{T}\Big)\Big(\partial_t v + v\partial_x v + \dfrac{\alpha-1}{\alpha} g\partial_x\zeta\Big) + \dfrac{1}{\alpha}\partial_x\zeta + \dfrac{2}{45}\partial_x^4\Big((1+\alpha\mathcal{T}[0])^{-1}(g\partial_x\zeta)\Big) \\
\quad + \dfrac{2}{3}\partial_x((\partial_x v)^2) + \dfrac{2}{3}\zeta\partial_x^2\Big((1+\alpha\mathcal{T}[0])^{-1}(g\partial_x\zeta)\Big) + \partial_x\zeta\partial_x\Big((1+\alpha\mathcal{T}[0])^{-1}(g\partial_x\zeta)\Big) = 0,
\end{cases}
\tag{2.17}
$$

where $h = h_0 + \zeta$. Following the same techniques as for the derivation of (2.14), one obtains the dispersion relation for (2.17):

$$
\tilde{w}^2_{\alpha,eB} = \frac{gh_0k^2\Big(1 + \dfrac{(\alpha-1)}{3}k^2 + \dfrac{k^4}{45}(\alpha - 1 + \frac{2}{1+\frac{\alpha k^2}{3}})\Big)}{\Big(1 + \dfrac{\alpha}{3}k^2 + \dfrac{\alpha}{45}k^4\Big)}.
\tag{2.18}
$$

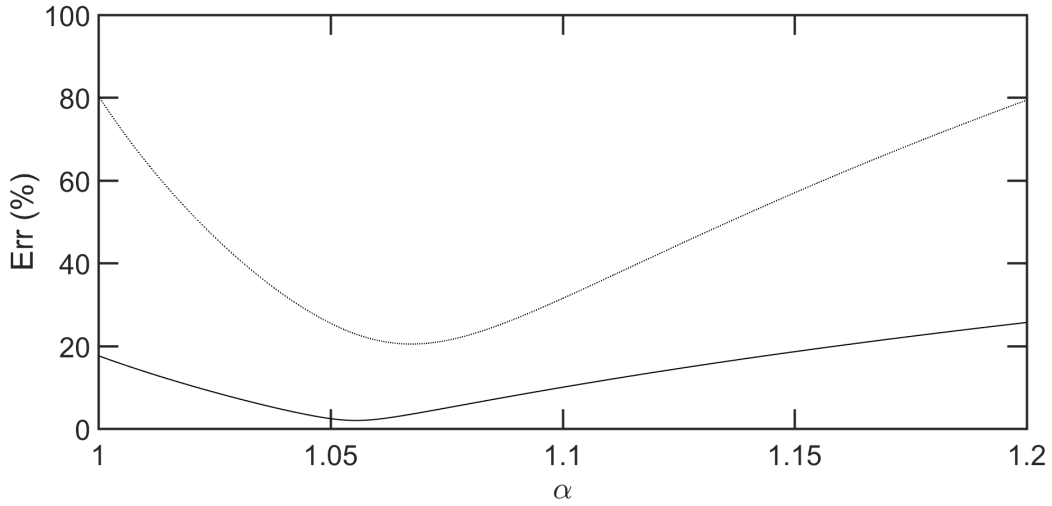

FIGURE 4. Phase and group velocities weighted averaged error as a function of α for $0 \leq k \leq 10$. The model (2.17) is in solid line, the Green-Naghdi model in the Camssa-Holm regime (GN-CH) [3] is in dots.

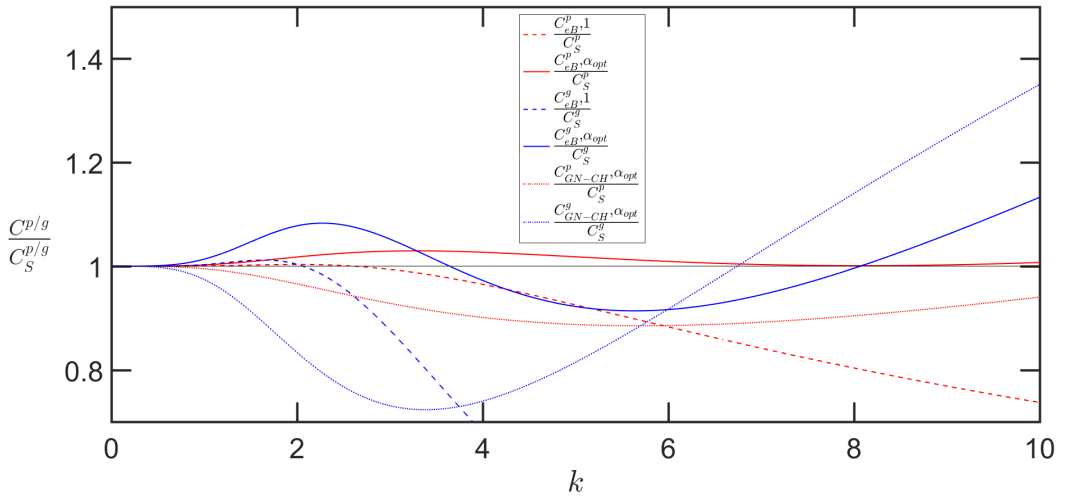

FIGURE 5. Errors on linear phase velocity (red) and group velocity (blue). The reference from Stokes theory (black solid line), the eB model (2.17) ($\alpha = 1.0555$) in solid lines, the eB model (2.17) ($\alpha = 1$) in dashes, the GN-CH model [3] ($\alpha = 1.0670$) in dots.

At this stage, one has to minimize the error function (2.16) for $\tilde{w}^2_{\alpha,eB}$ defined in (2.18). In Figure 4 we plot the related error in terms of α. One can see clearly that that the smallest value of the weighted averaged error ($\approx 2\%$) over the dispersive range $0 \leq k \leq 10$ is reached at $\alpha = 1.0555$, while the absolute minimum of the weighted averaged error associated with the Green-Naghdi model in the Camassa-Holm regime (GN-CH) (precise up to $\mathcal{O}(\mu^2, \mu\varepsilon^2)$) [3] is much larger ($\approx 20\%$). In Figure 5, errors on linear phase (red) and group (blue) velocities are plotted. The ratio $\dfrac{C^p_{eB,\alpha_{opt}}}{C^p_S}$ with an optimal choice $\alpha = 1.0555$ (red solid line) is very close to the reference from Stokes theory (black solid line) which shows a very good correspondence between the dispersion relation obtained using model (2.17) with $\alpha = 1.0555$ and the theoretical one over $0 \leq k \leq 10$. Larger difference exist between the group velocity (blue solid line) and the reference from Stokes theory (black solid line). This difference starts to proliferate when

$K > 10$, showing an overestimation of this property. When the modelled dispersion relation is obtained using the GN-CH model [3] with $\alpha = 1.0670$ a clear discrepancy exists for both linear group and phase velocity errors (blue and red dot lines). From here, one can deduce the significant improvement in the dispersive properties of model (2.17) with an appropriate choice of α_{opt} in the large frequency regime. In conclusion, the Green-Naghdi equations in the Camassa-Holm regime (precise up to $\mathcal{O}(\mu^2, \mu\varepsilon^2)$) are restrictive due to the sole inclusion of weak dispersion and nonlinearity. This usually restrain precise applications inside the surf area. The eB model (2.17) contains higher-order dispersive terms and an adjustable parameter α which enlarge the application scope remarkably to cover the area from deep water (long wavelength regime) into the area of breaking waves (short wavelength regime *i.e.* high frequency), see numerical test in section 4.3.

2.4. **Stability of the extended Boussinesq models.** The standard Boussinesq system is not stable in high frequency regime due to the third order derivatives in ζ that are involved in the model. One can see for instance [3], where the high frequency instabilities of an improved GN-CH model are studied. These instabilities are due to the third order derivative existing in the equation. One of the advantages of the eB is its stability in high frequency regime due to the presence of higher order derivatives, namely derivatives of order five in ζ. These terms seems to have a stabilizing effect. In what follows, we discuss qualitatively the stability of both models (2.11) and (2.17).

2.4.1. *Stability of the extended Boussinesq model with high order derivatives.* Before discussing the stability of the eB models in high frequency regime, we would like to mention that the choice of α in the model (2.11) in high frequency regime does not play an important role. In fact the latter model has poor dispersive properties in intermediate and large wave numbers regime, see discussion in section 2.3. Therefore, one has to choose $\alpha = 1$.

The system of equations (2.11) with $\alpha = 1$ reads:

$$\begin{cases} \partial_t\zeta + \partial_x\big(hv\big) \;=\; 0, \\ \Big(1 + \mathcal{T}[0] - \mathfrak{T}\Big)\Big(\partial_t v + v\partial_x v\Big) + g\partial_x\zeta + \dfrac{2}{45}g\partial_x^5\zeta + \dfrac{2}{3}\partial_x((\partial_x v)^2) \\ \quad + \dfrac{2}{3}g\zeta\partial_x^3\zeta + g\partial_x\zeta\partial_x^2\zeta = 0, \end{cases} \tag{2.19}$$

where $h = h_0 + \zeta$. We carry out the linear behaviour examination of slight perturbation $(\tilde{\zeta}, \tilde{v})$ of a steady state solution $(\underline{\zeta}, \underline{v})$. These perturbations are governed by the following linear system of equations:

$$\begin{cases} \partial_t\tilde{\zeta} + (h_0 + \underline{\zeta})\partial_x\tilde{v} + \underline{v}\partial_x\tilde{\zeta} \;=\; 0, \\ \Big(1 + \mathcal{T}[0] - \mathfrak{T}\Big)\Big(\partial_t\tilde{v} + \underline{v}\partial_x\tilde{v}\Big) + g\partial_x\tilde{\zeta} + \dfrac{2}{45}g\partial_x^5\tilde{\zeta} + \dfrac{2}{3}g\underline{\zeta}\partial_x^3\tilde{\zeta} = 0. \end{cases} \tag{2.20}$$

Going in search for plane wave solution of the above system, one can derive the corresponding dispersion relation. These solutions are of the form $(\tilde{\zeta}; \tilde{v}) = e^{i(kx - wt)}(\underline{\zeta}, \underline{v})$ and the dispersion relation is the following:

$$\frac{(w - k\underline{v})^2}{g(h_0 + \underline{\zeta})k^2} = \frac{\Big(1 - \dfrac{2}{3}k^2\underline{\zeta} + \dfrac{2}{45}k^4\Big)}{\Big(1 + \dfrac{1}{3}k^2 + \dfrac{1}{45}k^4\Big)}. \tag{2.21}$$

The perturbations of the rest state $(\underline{\zeta}, \underline{v}) = (0, 0)$ are always stable as per the below dispersion relation:

$$w^2 = \frac{gh_0k^2\Big(1 + \dfrac{2}{45}k^4\Big)}{\Big(1 + \dfrac{1}{3}k^2 + \dfrac{1}{45}k^4\Big)}. \tag{2.22}$$

However, a quick functional study shows that the numerator of the right-hand side of (2.21) becomes negative whenever $\underline{\zeta} > \dfrac{2k^4 + 45}{30k^2}$. Thus, as provided by (2.21), w remains real for large wavenumbers, under the condition that $\underline{\zeta} < \dfrac{2k^4 + 45}{30k^2}$. In the majority of the applications we have in mind, the overall surface deformation $\underline{\zeta}$ does not go beyond $\dfrac{2k^4 + 45}{30k^2}$, and this condition is satisfied. Actually, as k gets

large (i.e in high frequency regime), the upper bound of $\underline{\zeta}$ gets also large ($\approx \frac{k^2}{15}$), hence extending the range of values of the overall surface deformation $\underline{\zeta}$ for which the condition is satisfied. This ensure a numerical stability in most of the situations considered for applications (see Figure 6).

Remark 2.23. Replacing $\partial_x^5\zeta$ by $\partial_x^4\Big((1+\mathcal{T}[0])^{-1}(\partial_x\zeta)\Big)$ in the second equation of (2.19), one gets the following model:

$$\begin{cases} \partial_t\zeta + \partial_x\big(hv\big) \;=\; 0, \\ \Big(1+\mathcal{T}[0]-\mathfrak{T}\Big)\Big(\partial_t v + v\partial_x v\Big) + g\partial_x\zeta + \frac{2}{45}g\partial_x^4\Big((1+\mathcal{T}[0])^{-1}(\partial_x\zeta)\Big) + \frac{2}{3}\partial_x((\partial_x v)^2) \\ \quad + \frac{2}{3}g\zeta\partial_x^3\zeta + g\partial_x\zeta\partial_x^2\zeta = 0. \end{cases} \tag{2.24}$$

This replacement modifies the dispersion relation (2.21) into:

$$\frac{(w-k\underline{v})^2}{g(h_0+\underline{\zeta})k^2} = \frac{\Big(1-\frac{2}{3}k^2\underline{\zeta}+\frac{k^4}{45}\big(\frac{2}{1+\frac{1}{3}k^2}\big)\Big)}{\Big(1+\frac{1}{3}k^2+\frac{1}{45}k^4\Big)}. \tag{2.25}$$

A similar functional study to the previous one shows that the r.h.s numerator of (2.25) is negative whenever $\underline{\zeta} > \frac{2k^4+15k^2+45}{10k^4+30k^2}$. In high frequency regime, the upper bound of the overall surface deformation $\underline{\zeta}$ is approximately close to 0.2, hence reducing the range of values of $\underline{\zeta}$ for which the condition is satisfied, namely $-h_0 < \underline{\zeta} < 0.2$ (keeping mind that $h = h_0 + \underline{\zeta}$ should remain always positive). Therefore, if this condition is not satisfied the complex square root of w will generate an instability in the model. Actually, a stability in high frequency regime is ensured if the condition $-h_0 < \underline{\zeta} < 0.2$ is satisfied which we believe is a limitation for the applications that we have in mind. Thus, one can deduce that factorizing only the fifth order derivative present in the second equation of (2.19) does not stabilize the model, at least for a big range of values of the overall surface deformation $\underline{\zeta}$ (see Figure 6). This is why we suggested in section 2.2 to factorize second, third and fifth order derivatives present in the second equation of (2.19). The stability of the eB model with factorized high order derivatives (2.17) is discussed in the next subsection.

2.4.2. *Stability of the extended Boussinesq model with factorized high order derivatives.* In what follows, we explore the stability of the eB model with factorized high order derivatives (2.17). When linearizing (2.17) about a non steady state, one gets:

$$\frac{(w-k\underline{v})^2}{g(h_0+\underline{\zeta})k^2} = \frac{\Big(1+\frac{(\alpha-1)k^2}{3}-\frac{2k^2\underline{\zeta}}{3(1+\frac{\alpha}{3}k^2)}+\frac{(\alpha-1)k^4}{45}+\frac{2k^4}{45(1+\frac{\alpha}{3}k^2)}\Big)}{\Big(1+\frac{\alpha}{3}k^2+\frac{\alpha}{45}k^4\Big)}. \tag{2.26}$$

The *r.h.s* numerator in (2.26) is positive if and only if

$$\underline{\zeta} < \frac{k^2\left(\alpha\left((\alpha-1)k^2+15\alpha-12\right)+3\right)+90\alpha-45}{90} + \frac{3}{2k^2}.$$

We recall that $\alpha > 1$. Indeed, improving the dispersive properties of the model (2.17) in large frequency regime requires an appropriate choice $\alpha = 1.0555$ (see discussion in section 2.3). With this choice of α and in high frequency regime, the *r.h.s* of the above inequality becomes very large, namely same order as $\frac{\alpha(\alpha-1)k^4}{90}$. Thus, relaxing the stability condition on $\underline{\zeta}$. For the numerical tests, we choose to work with the model (2.17) which appears to be stable.

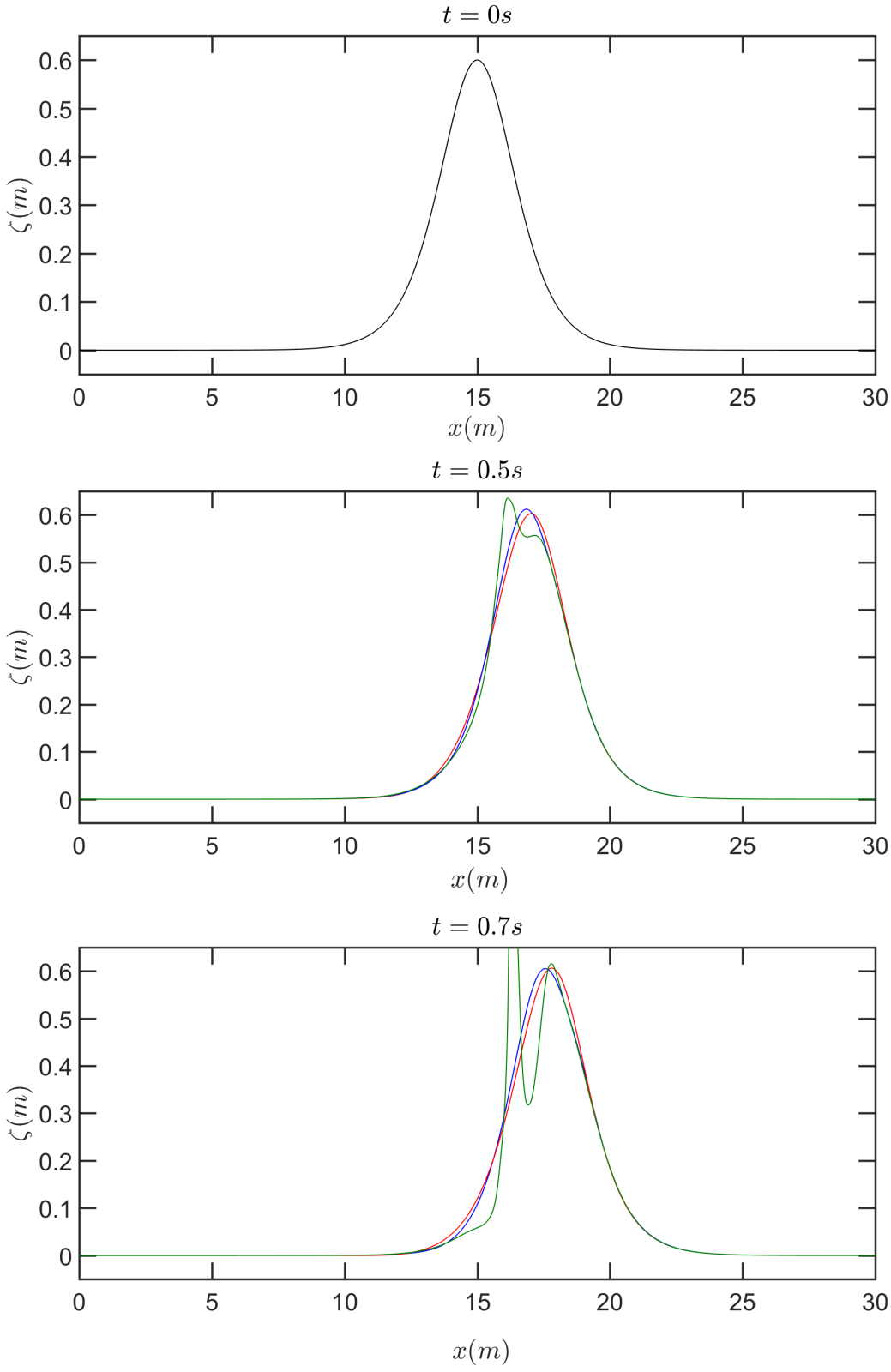

FIGURE 6. Comparison at different times between the solutions of the models (2.19) (blue line), (2.17) (red line) and (2.24) (green line) in high frequency regime.

Figure 6 shows clearly the stability of the eB models (2.19) and (2.17) while the model (2.24) seems to be unstable in high frequency regime. In fact, when implementing in model (2.24) an initial solution

that does not satisfy the limiting stability condition discussed in remark 2.23, more precisely when choosing $\underline{\zeta} = 0.6 > 0.2$, one observes a high frequency instability. We would like to mention that we tried the same test but starting with an initial solution where the overall surface deformation is $\underline{\zeta} = 0.1$. All models seems to be stable but we do not include this test here for the sake of simplicity. Thus, one can deduce that factorizing only the fifth order derivative present in the second equation of (2.19) does not stabilize the model, at least for a big range of values of the overall surface deformation $\underline{\zeta}$. This is the reason why, for the rest of the paper, we choose to work with the model (2.17), where high order derivatives are factorized which, as seen above, is always stable. Of course, one could use model (2.19) which seems to be stable, but at the price of loosing the improved dispersive properties that model (2.17) enjoys, see section 2.3 and test case of section 4.3.

3. Numerical methods

In what follows, we will just introduce the numerical scheme devoted to solve the eB model with factorized high order derivatives (2.10) in order to ease the reading. A similar numerical scheme is adopted when the eB model with high order derivatives (2.6) is concerned.

This class of models has two main components, hyperbolic and dispersive. This remarkable structure makes them suitable for the implementation of a hybrid scheme splitting the two main components of the equations. This strategy has been initially introduced for Boussinesq-like and Green-Naghdi equations in order to handle correctly wave breaking that occurs as waves approach the shore, see [2, 9, 17, 18, 27]. A computation of a half-time step of the hyperbolic part is used as a sensor to evaluate the energy loss occurring during wave breaking (accurate detection of wave fronts), see [42]. Near the breaking points, the dynamics of the waves are described correctly using the hyperbolic part but the dispersive components of the equation become very singular. In order to handle wave breaking, switching from the dispersive part to the hyperbolic part is indispensable. In this paper, we do not investigate breaking waves. In fact, our work is limited to the flat topography case and we leave for future research the treatment of breaking waves in the variable bottom configuration. However, we stick here to the splitting strategy since it is computationally efficient, stable and cheap. The splitting scheme following the lines in [2, 27, 3] is presented in the section below.

3.1. The splitting scheme.

We recall first the eB system (2.10) under consideration:

(3.1)
$$\begin{cases} \partial_t\zeta + \partial_x\big(hv\big) \;=\; 0, \\ \Big(1+\varepsilon\alpha\mathcal{T}[0]-\varepsilon^2\alpha\mathfrak{T}\Big)\Big(\partial_t v+\varepsilon v\partial_x v+\dfrac{\alpha-1}{\alpha}\partial_x\zeta\Big)+\dfrac{1}{\alpha}\partial_x\zeta+\dfrac{2}{45}\varepsilon^2\partial_x^4\Big((1+\varepsilon\alpha\mathcal{T}[0])^{-1}(\partial_x\zeta)\Big) \\ \quad +\varepsilon^2\dfrac{2}{3}\partial_x((\partial_x v)^2)+\varepsilon^2\dfrac{2}{3}\zeta\partial_x^2\Big((1+\varepsilon\alpha\mathcal{T}[0])^{-1}(\partial_x\zeta)\Big)+\varepsilon^2\partial_x\zeta\partial_x\Big((1+\varepsilon\alpha\mathcal{T}[0])^{-1}(\partial_x\zeta)\Big)=\mathcal{O}(\varepsilon^3), \end{cases}$$

where $h = 1+\varepsilon\zeta$. The solution operator $S(.)$ related to (3.1) is decomposed at each time step Δt following a hybrid Strang splitting scheme:

$$S(\Delta t) = S_1(\Delta t/2)S_2(\Delta t)S_1(\Delta t/2).$$

- $S_1(t)$ is the solution operator related to the hyperbolic nonlinear shallow water equations, NSWE:

(3.2)
$$\begin{cases} \partial_t\zeta + \partial_x\big(hv\big) \;=\; 0, \\ \partial_t v+\varepsilon v\partial_x v+\dfrac{\alpha-1}{\alpha}\partial_x\zeta+\dfrac{1}{\alpha}\partial_x\zeta=0. \end{cases}$$

The NSWE system (3.2) can be written in the following conservative form:

(3.3)
$$\begin{cases} \partial_t\zeta + \partial_x\big(hv\big) \;=\; 0, \\ \partial_t v+\partial_x\Big(\dfrac{\varepsilon}{2}v^2+\zeta\Big)=0, \end{cases}$$

where $h = 1+\varepsilon\zeta$.

• $S_2(t)$ is the solution operator related to the remaining (dispersive) part of the equations.

$$\begin{cases} \partial_t \zeta \;=\; 0, \\ \Big(1+\varepsilon\alpha\mathcal{T}[0]-\varepsilon^2\alpha\mathfrak{T}\Big)\Big(\partial_t v-\dfrac{1}{\alpha}\partial_x\zeta\Big)+\dfrac{1}{\alpha}\partial_x\zeta+\dfrac{2}{45}\varepsilon^2\partial_x^4\Big((1+\varepsilon\alpha\mathcal{T}[0])^{-1}(\partial_x\zeta)\Big) \\ +\varepsilon^2\dfrac{2}{3}\partial_x((\partial_x v)^2)+\varepsilon^2\dfrac{2}{3}\zeta\partial_x^2\Big((1+\varepsilon\alpha\mathcal{T}[0])^{-1}(\partial_x\zeta)\Big)+\varepsilon^2\partial_x\zeta\partial_x\Big((1+\varepsilon\alpha\mathcal{T}[0])^{-1}(\partial_x\zeta)\Big)=0. \end{cases} \tag{3.4}$$

The hyperbolic conservative structure of system (3.3) allows a computation of S_1 following a finite-volume method. Whereas, a classical finite difference method is used to compute S_2.

3.2. **Finite volume scheme.** The hyperbolic system (3.3) is conveniently rewritten with conservative variables and a flux function:

$$\partial_t U+\partial_x(F(U))=0, \tag{3.5}$$

where,

$$U=\begin{pmatrix}\zeta\\ v\end{pmatrix},\quad F(U)=\begin{pmatrix}hv\\ \dfrac{\varepsilon}{2}v^2+\zeta\end{pmatrix}, \tag{3.6}$$

with $h=1+\varepsilon\zeta$. The Jacobian matrix is given by:

$$A(U)=d(F(U))=\begin{pmatrix}\varepsilon v & h\\ 1 & \varepsilon v\end{pmatrix}. \tag{3.7}$$

The homogeneous system (3.5) is strictly hyperbolic if $\inf\limits_{x\in\mathbb{R}} h>0$ that is to say the domain of the fluid must remain strictly connected.

The Cauchy problem associated to (3.5) is the following:

$$\begin{cases} \partial_t U+\partial_x(F(U)) \;=\; 0, \qquad t\geq 0, x\in\mathbb{R}. \\ U(0,x)=U_0(x), \qquad x\in\mathbb{R}. \end{cases} \tag{3.8}$$

The finite volume method used to the approximation of (3.8) imposes conservation laws in a one-dimensional control volume $[x_{i-1/2},x_{i+1/2}]\times[t^n,t^{n+1}]$ of dimensions $\Delta x=x_{i+1/2}-x_{i+1/2}$ and $\Delta t=t^{n+1}-t^n$.

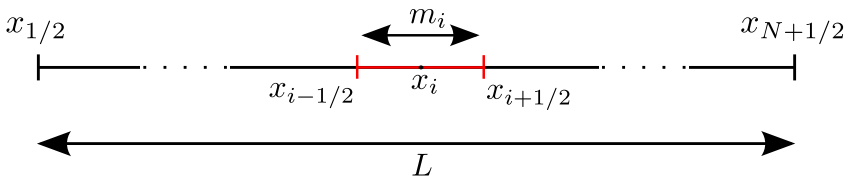

FIGURE 7. The space discretization.

The approximate cell average of U on the cell $m_i=[x_{i-1/2},x_{i+1/2}]$ at time t is denoted by $\overline{U}_i$ and given by:

$$\overline{U}_i=\frac{1}{\Delta x}\int_{m_i}U(t,x)\,dx\ .$$

The approximate cell average of U on the cell $m_i=[x_{i-1/2},x_{i+1/2}]$ at time t^n is denoted by $\overline{U}_i^n$ and given by:

$$\overline{U}_i^n=\frac{1}{\Delta x}\int_{m_i}U(t^n,x)\,dx\ .$$

Integrating (3.2) over the computational cell m_i, the semi-discrete form can be represented as:

$$\frac{d\overline{U}_i(t)}{dt}+\frac{1}{\Delta x}\Big(F_{i+1/2}-F_{i-1/2}\Big)=0 \tag{3.9}$$

where $F_{i\pm1/2}$ are the numerical fluxes defined at each cell interface as:

$$F_{i+1/2} = \widetilde{F}(\overline{U}_i, \overline{U}_{i+1}) \approx \frac{1}{\Delta x}\int_{m_i} F(U(t, x_{i+1/2}))dx. \tag{3.10}$$

The computation of high-order accurate numerical fluxes is reached by reconstructing left and right constant averaged values using a fifth-order WENO scheme, before applying the numerical flux.

3.2.1. *High order finite-volume scheme: WENO5-RK4.* Fixed stencil interpolation of high order accuracy (second or higher) may not be adequate and thus *oscillatory* near a discontinuity. In nonlinear problems containing discontinuities, such oscillations usually leads to numerical instabilities. Reaching high order accuracy in smooth regions while avoiding the spurious ossicllations around discontinuity can be achieved by using a fifth-order accuracy WENO reconstruction for hyperbolic conservation laws, following [21, 40]. Problems with piecewise smooth solutions containing discontinuities can be solved using the appropriately-designed high order accurate WENO schemes. The main idea lies at the approximation stage, where a nonlinear adaptive stencil is used in the reconstruction procedure following a convex combination of all candidate stencils instead of just one to achieve the essentially non-oscillatory property. A proper weight is assigned to each of the candidate stencils determining its contribution to the final approximation. In fact, a nearly zero weight is assigned to the stencils which contain the discontinuities. Second-order schemes tend to alter the dispersive properties of the model due to dispersive truncation errors. To prevent this in the study of dispersive waves, high order schemes are imperative [2, 9, 27]. Using the same reconstruction method proposed in [2, 3], we consider a cell m_i, and the corresponding constant averaged value $\overline{U}_i^n = (\overline{\zeta}_i^n, \overline{v}_i^n)$. Consequently, high order reconstructed left and right values $\overline{U}_i^{n,-}$ and $\overline{U}_i^{n,+}$, built following the five points stencil, are introduced as follows:

$$\overline{U}_i^{n,+} = \overline{U}_i^n + \frac{1}{2}\overline{\delta U}_i^{n,+} \quad \text{and} \quad \overline{U}_i^{n,-} = \overline{U}_i^n - \frac{1}{2}\overline{\delta U}_i^{n,-}, \tag{3.11}$$

where $\overline{\delta U}_i^{n,+}$ and $\overline{\delta U}_i^{n,-}$ are defined as follows:

$$\begin{aligned}\overline{\delta U}_i^{n,+} &= \frac{2}{3}(\overline{U}_{i+1}^n - \overline{U}_i^n) + \frac{1}{3}(\overline{U}_i^n - \overline{U}_{i-1}^n) - \frac{1}{10}(-\overline{U}_{i-1}^n + 3\overline{U}_i^n - 3\overline{U}_{i+1}^n + \overline{U}_{i+2}^n)\\ &\quad -\frac{1}{15}(-\overline{U}_{i-2}^n + 3\overline{U}_{i-1}^n - 3\overline{U}_i^n + \overline{U}_{i+1}^n)\end{aligned} \tag{3.12}$$

$$\begin{aligned}\overline{\delta U}_i^{n,-} &= \frac{2}{3}(\overline{U}_i^n - \overline{U}_{i-1}^n) + \frac{1}{3}(\overline{U}_{i+1}^n - \overline{U}_i^n) - \frac{1}{10}(-\overline{U}_{i-2}^n + 3\overline{U}_{i-1}^n - 3\overline{U}_i^n + \overline{U}_{i+1}^n)\\ &\quad -\frac{1}{15}(-\overline{U}_{i-1}^n + 3\overline{U}_i^n - 3\overline{U}_{i+1}^n + \overline{U}_{i+2}^n).\end{aligned} \tag{3.13}$$

The coefficients $\frac{2}{3}$, $\frac{1}{3}$, $\frac{-1}{10}$ and $\frac{-1}{15}$ are set for better dissipation and dispersion properties in the truncature error. As a result, the modified scheme becomes the following:

$$\overline{U}_i^{n+1} = \overline{U}_i^n - \frac{\Delta t}{\Delta x}\Big(\widetilde{F}(\overline{U}_i^{n,+}, \overline{U}_{i+1}^{n,-}) - \widetilde{F}(\overline{U}_{i-1}^{n,+}, \overline{U}_i^{n,-})\Big). \tag{3.14}$$

At this point, it is important to apply a limitation procedure to prevent oscillations near discontinuities. To this end, we use the same limitation strategy as in [2, 3]. Consequently, scheme (3.14) becomes

$$\overline{U}_i^{n+1} = \overline{U}_i^n - \frac{\Delta t}{\Delta x}\Big(\widetilde{F}({}^L\overline{U}_i^{n,+}, {}^L\overline{U}_{i+1}^{n,-}) - \widetilde{F}({}^L\overline{U}_{i-1}^{n,+}, {}^L\overline{U}_i^{n,-})\Big). \tag{3.15}$$

The limited high-order reconstructed values are defined as follows:

$${}^L\overline{U}_i^{n,+} = \overline{U}_i^n + \frac{1}{2}L_i^+(\overline{U}^n) \quad \text{and} \quad {}^L\overline{U}_i^{n,-} = \overline{U}_i^n - \frac{1}{2}L_i^-(\overline{U}^n). \tag{3.16}$$

These reconstructions must be performed on both conservative variables $\overline{U}_i^n = (\overline{\zeta}_i^n, \overline{v}_i^n)$.

$L_i^+(\overline{U}^n)$ and $L_i^-(\overline{U}^n)$ are defined, using the following limiter,

$$L(u,v,w) = \begin{cases} min(|u|, |v|, 2|w|)\ sgn(u) & \text{if} \quad sgn(u) = sgn(v),\\ 0 \quad \text{else.}\end{cases} \tag{3.17}$$

Depending on (3.17), we define the limiting process as,

$$L_i^+(\overline{U}^n) = L(\delta\overline{U}_i^n, \delta\overline{U}_{i+1}^n, \overline{\delta U}_i^{n,+}) \quad \text{and} \quad L_i^-(\overline{U}^n) = L(\delta\overline{U}_{i+1}^n, \delta\overline{U}_i^n, \overline{\delta U}_i^{n,-}),$$

with $\delta\overline{U}_{i+1}^n = \overline{U}_{i+1}^n - \overline{U}_i^n$ and $\delta\overline{U}_i^n = \overline{U}_i^n - \overline{U}_{i-1}^n$ are upstream and downstream variations, and $\overline{\delta U}_i^{n,+}$ and $\overline{\delta U}_i^{n,-}$ taken from (3.12) and (3.13).

Remark 3.18. At this stage, it is worth mentioning that steady states solution $\zeta = \text{cst}$ and $v = 0$ are preserved at the discrete level.

Regarding time discretization, fourth-order explicit Runge–Kutta "RK4" method is used, we describe it in what follows. Given the ODE $\dfrac{dy}{dt} = f(t, y)$, one has,

$$\begin{aligned} k_1 &= f(t^n, y^n), \\ k_2 &= f(t^n + \frac{\Delta t}{2}, y^n + \Delta t\frac{k_1}{2}), \\ k_3 &= f(t^n + \frac{\Delta t}{2}, y^n + \Delta t\frac{k_2}{2}), \\ k_4 &= f(t^n + \Delta t, y^n + \Delta t k_3), \\ y^{n+1} &= y^n + \frac{\Delta t}{6}\big(k_1 + 2k_2 + 2k_3 + k_4\big). \end{aligned} \tag{3.19}$$

Applying (3.19) to (3.15), one gets the "WENO5-RK4" scheme.

3.3. **Finite difference scheme for the dispersive part.** The splitting scheme is a mix between a finite volume discretization and a finite difference method. This mix induces a switching between cell-averaged values defined by the finite volume discretization and nodal values used by the finite difference discretization for each unknown and at each time step. Using fifth-order accuracy WENO reconstruction, one can approximate the nodal values (i.e finite difference unknowns) $(U_i^n)_{i=1,N+1}$ in terms of the cell-averaged values (i.e finite volume unknowns) $(\overline{U}_i^n)_{i=1,N}$ by the following relation:

$$U_i^n = \frac{1}{30}\overline{U}_{i-2}^n - \frac{13}{60}\overline{U}_{i-1}^n + \frac{47}{60}\overline{U}_i^n + \frac{9}{20}\overline{U}_{i+1}^n - \frac{1}{20}\overline{U}_{i+2}^n + \mathcal{O}(\Delta x^5), \quad 1 \le i \le N+1, \tag{3.20}$$

The global order of the scheme is preserved. In fact, the formula is precise up to order $\mathcal{O}(\Delta x^5)$ terms. Before proceeding by the computation of S_2, we recall first the remaining (dispersive part) of the equations, given in section 3.1.

$$\begin{cases} \partial_t\zeta = 0, \\ \Big(1 + \varepsilon\alpha\mathcal{T}[0] - \varepsilon^2\alpha\mathfrak{T}\Big)\Big(\partial_t v - \dfrac{1}{\alpha}\partial_x\zeta\Big) + \dfrac{1}{\alpha}\partial_x\zeta + \dfrac{2}{45}\varepsilon^2\partial_x^4\Big((1 + \varepsilon\alpha\mathcal{T}[0])^{-1}(\partial_x\zeta)\Big) \\ +\varepsilon^2\dfrac{2}{3}\partial_x((\partial_x v)^2) + \varepsilon^2\dfrac{2}{3}\zeta\partial_x^2\Big((1 + \varepsilon\alpha\mathcal{T}[0])^{-1}(\partial_x\zeta)\Big) + \varepsilon^2\partial_x\zeta\partial_x\Big((1 + \varepsilon\alpha\mathcal{T}[0])^{-1}(\partial_x\zeta)\Big) = 0. \end{cases} \tag{3.21}$$

Using an explicit Euler in time scheme, the finite discretization of the system (3.21) using classical finite difference methods leads to the following discrete problem:

$$\begin{cases} \dfrac{\zeta^{n+1} - \zeta^n}{\Delta t} = 0, \\ \dfrac{v^{n+1} - v^n}{\Delta t} - \dfrac{1}{\alpha}D_1(\zeta^n) + \Big(I - \dfrac{\varepsilon\alpha}{3}D_2 + \dfrac{\varepsilon^2\alpha}{45}D_4\Big)^{-1}\Big[\dfrac{1}{\alpha}D_1(\zeta^n) + \dfrac{2}{45}\varepsilon^2 D_4\Big(\big(1 - \dfrac{\varepsilon\alpha}{3}D_2\big)^{-1}(D1(\zeta^n))\Big) \\ +\varepsilon^2\dfrac{2}{3}D_1((D_1v^n)^2) + \varepsilon^2\dfrac{2}{3}\zeta^n D_2\Big(\big(1 - \dfrac{\varepsilon\alpha}{3}D_2\big)^{-1}(D1(\zeta^n))\Big) + \varepsilon^2 D_1(\zeta^n)D_1\Big(\big(1 - \dfrac{\varepsilon\alpha}{3}D_2\big)^{-1}(D1(\zeta^n))\Big)\Big] = 0. \end{cases} \tag{3.22}$$

The matrices D_1, D_2 and D_4 are respectively the classical centered discretizations of the derivatives ∂_x, ∂_x^2, and ∂_x^4 given below. The spatial derivatives are discretized using fourth-order formulae, "DF4":

$$(\partial_x U)_i = \frac{1}{12\Delta x}(-U_{i+2} + 8U_{i+1} - 8U_{i-1} + U_{i-2}),$$

$$(\partial_x^2 U)_i = \frac{1}{12\Delta x^2}(-U_{i+2} + 16U_{i+1} - 30U_i + 16U_{i-1} - U_{i-2}),$$

$$(\partial_x^4 U)_i = \frac{1}{6\Delta x^4}(-U_{i+3} + 12U_{i+2} - 39U_{i+1} + 56U_i - 39U_{i-1} + 12U_{i-2} - U_{i-3}).$$

A standard extension to fourth-order classical Runge-Kutta "RK4" scheme is used, and thus one obtains the "DF4-RK4" scheme.

Remark 3.23. At this stage, it is worth mentioning that the numerical scheme of the eB system with high order derivatives (2.6) is similar to the one developed for model (2.10). In fact, the hyperbolic part of the system is the same as in (3.2), but the high order derivatives involved in the second equation of the remaining (dispersive) part should be treated accordingly. More precisely, third and fifth order derivatives are discretized using the following fourth-order formulae:

$$(\partial_x^3 U)_i = \frac{1}{8\Delta x^3}(-U_{i+3} + 8U_{i+2} - 13U_{i+1} + 13U_{i-1} - 8U_{i-2} + U_{i-3}),$$

$$(\partial_x^5 U)_i = \frac{1}{6\Delta x^5}(-U_{i+4} + 9U_{i+3} - 26U_{i+2} + 29U_{i+1} - 29U_{i-1} + 26U_{i-2} - 9U_{i-3} + U_{i-4}).$$

3.4. **Boundary conditions.** To close the differential problems, boundary conditions need to be imposed. Boundary conditions for both the hyperbolic and dispersive parts of the splitting scheme are treated by imposing suitable relations on both cell-averaged and nodal quantities. In this paper, we only consider periodic boundary conditions as it was already done in [4] for the study of internal waves.

For the hyperbolic part, "Ghosts" cells are introduced respectively at the western and eastern boundaries of the domain. The imposed relations on the cell-averaged quantities are the following:

• $\overline{U}_{-k+1} = \overline{U}_{N-k+1}$, and $\overline{U}_{N+k} = \overline{U}_k$, $k \geq 1$, for periodic conditions on western and eastern boundaries.

For the dispersive part, we simply impose the boundary conditions on the nodal values located outside of the domain. In this way, we maintain centered formula at the boundaries, while keeping a regular structure in the discretized model:

• $U_{-k+1} = U_{N-k+1}$, and $U_{N+k} = U_k$, $k \geq 1$, for periodic conditions on western and eastern boundaries.

4. Numerical validations

This part is devoted to the numerical validations of the model and the numerical scheme.

We begin by studying the propagation of a solitary wave solution with correctors of order $\mathcal{O}(\varepsilon^3)$ established in [23]. We compare our numerical solution with an analytic one (up to an $\mathcal{O}(\varepsilon^3)$ remainder) at several times and show that our numerical scheme is very efficient and accurate.

Secondly, as usual when dealing with a model in oceanographical science, one has to test the ability of the model and the numerical method for the test of a head on collision of counter propagating solitary waves. A very good agreement is observed.

An important fact to reveal is whether or not the improved model is pertinent. The third numerical test reveals that in presence of large wave number, the choice of the parameter α and the high order derivatives factorization are crucial.

The fourth numerical test shows a very good agreement of the proposed extended Boussinesq model and the Green-Naghdi model proposed by Duchêne *et al.* [13]

The fifth test is build to test the ability of the model and the numerical method to deal with irregular solution. A very good behaviour is observed.

4.1. **Propagation of a solitary wave solution with correctors.** A careful examination revealed that the extended Boussinesq system (1.5) does not admit an exact solitary wave solution, see [23, Section 4]. In order to validate our numerical scheme we use the explicit solution with correctors of order $\mathcal{O}(\varepsilon^3)$ found in [23, Section 5] that we disclose below. Such solitary waves are analytical solutions of the extended Boussinesq system (1.5) up to $\mathcal{O}(\varepsilon^3)$ remainders. Therefore, this family of solutions can be used as a validation tool for our present numerical scheme and its given by (ζ, v) with

$$\zeta = \zeta_1 + \frac{\varepsilon^2}{2}\Big[(\zeta_2^0 + v_2^0)(x-t) + (\zeta_2^0 - v_2^0)(x+t) + \int_0^t f(s, x-t+s)ds - \int_0^t f(s, x+t-s)ds\Big], \tag{4.1}$$

and

$$v = v_1 + \frac{\varepsilon^2}{2}\Big[(\zeta_2^0 + v_2^0)(x-t) - (\zeta_2^0 - v_2^0)(x+t) + \int_0^t f(s, x-t+s)ds + \int_0^t f(s, x+t-s)ds\Big], \tag{4.2}$$

where (ζ_1, v_1) is the well known explicit solution of solitary travelling wave of the standard Boussinesq system (1.4) given by:

$$\begin{cases} \zeta_1(t,x) = a\ \mathrm{sech}^2\Big(k\ (x-ct)\Big)\ , \\ v_1(t,x) = \dfrac{c\zeta_1(t,x)}{1+\varepsilon\zeta_1(t,x)}\ , \end{cases}$$

where $k = \sqrt{\dfrac{3a}{4}}$ and $c = \sqrt{\dfrac{1}{1-a\varepsilon}}$ and a is an arbitrary chosen constant. The initial conditions ζ_2^0 and v_2^0 are both given in $C^\infty(\mathbb{R})$ and set $\zeta_2^0 = v_2^0 = \exp\Big(-\Big(\dfrac{3\pi x}{10}\Big)^2\Big)$. The function $f(t,x)$ is defined by:

$$f(\zeta_1, v_1) = \partial_x\zeta_1\partial_x\partial_t v_1 + \frac{2}{3}\zeta_1\partial_x^2\partial_t v_1 + \frac{1}{45}\partial_x^4\partial_t v_1 + \frac{1}{3}\partial_x\big(v_1(v_1)_{xx} - (v_1)_x^2\big).$$

In this test, we investigate the left to right propagation of a solitary wave initially centred at $x_0 = 20$, of relative amplitude $a = 0.2$. The computational domain length is $L = 100$ and discretized with 1600 cells. The solitary wave is initially far from boundaries, thus the periodic boundary conditions do not affect the computation. We compare the water surface profile of our numerical solution provided by the model (2.10) with $\varepsilon = 0.01$ and $\alpha = 1$, with the analytical one given by (4.1)-(4.2) at several times using the fifth order discretization "WENO5-DF4-RK4". An excellent agreement between numerical and analytical solutions is observed in Figure 8. The amplitude and shape of the computed solitary wave are accurately preserved during the propagation, indicating an accurate discretization of the governing equations in both space and time.

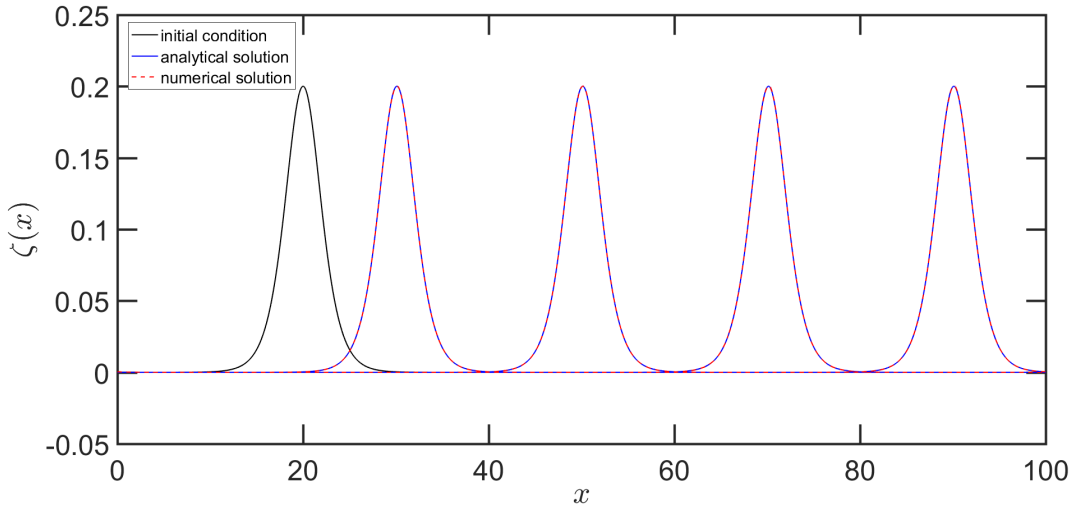

FIGURE 8. Propagation of a solitary wave: water surface profiles at $t = 0, 10, 30, 50$ and 70.

To complete the picture and assess the convergence of our numerical scheme, we compute the numerical solution for this particular test case for an increasing number of cells N, over a duration $T = 1$. We start with $N = 400$ number of cells and successively multiply the number of cells by two. The relative errors $E_{L^2}(\zeta)$ and $E_{L^2}(v)$ on the water surface deformation and the averaged velocity are computed at $t = 1$, using the discrete L^2 norm $\|.\|_2$:

$$E_{L^2}(\zeta) = \frac{\|\zeta_{num} - \zeta_{sol}\|_2}{\|\zeta_{sol}\|_2}; \qquad E_{L^2}(v) = \frac{\|v_{num} - v_{sol}\|_2}{\|v_{sol}\|_2}, \tag{4.3}$$

where (ζ_{num}, v_{num}) are the numerical solutions and (ζ_{sol}, v_{sol}) are the analytical ones coming from (4.1)-(4.2).

N	$E_{L^2}(\zeta)$	$E_{L^2}(v)$
400	3.50×10^{-3}	3.33×10^{-3}
800	9.32×10^{-4}	8.29×10^{-4}
1600	2.05×10^{-4}	1.70×10^{-4}
3200	3.23×10^{-5}	2.48×10^{-5}
6400	4.79×10^{-6}	3.50×10^{-6}
12800	1.44×10^{-6}	1.49×10^{-6}

TABLE 1. Propagation of a solitary wave: relative L^2-error table for the conservative variables.

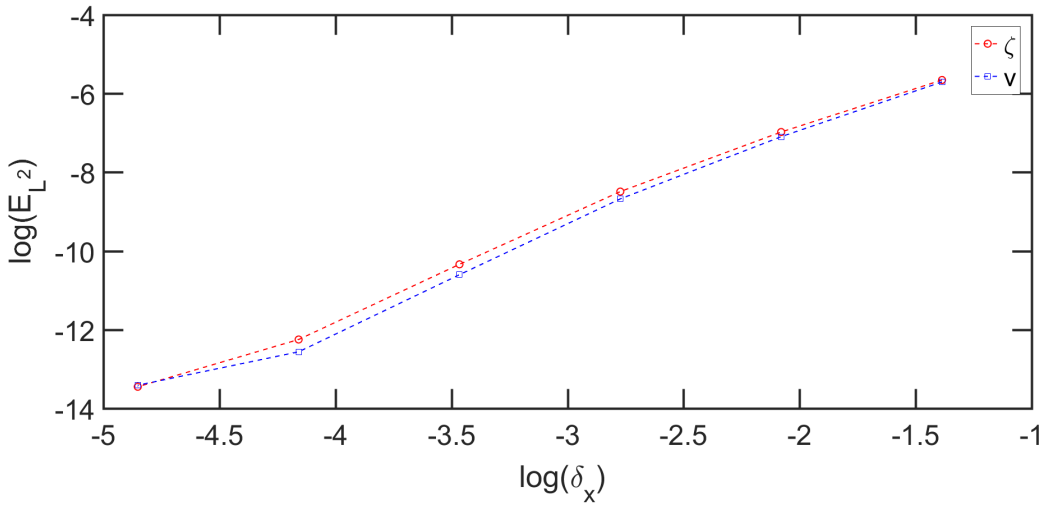

FIGURE 9. Propagation of a solitary wave: L^2-error on the water surface deformation and the averaged velocity for $a = 0.2$.

Results are presented in Table 1 and Figure 9 where $E_{L^2}(\zeta)$ and $E_{L^2}(v)$ are plotted against $\delta_x = \dfrac{L}{N}$ in log scales, for the considered relative amplitude $a = 0.2$. Very accurate results are obtained, indicating that the employed numerical method is capable of computing in a stable way the propagation of the a solitary wave. Moreover, computing a linear regression on all points yields a slope equal to 2.33 for ζ and 2.34 for the averaged velocity v.

Remark 4.4. We believe that the main reason for not obtaining the predicted order in space discretization is due to the fact that the analytic solution given in (4.1)-(4.2) satisfies the model (2.10) up to $\mathcal{O}(\varepsilon^3)$ remainders, that is to say it is an approximate solution. A remedy for this situation could be through calculating explicitly the $\mathcal{O}(\varepsilon^3)$ remainders by injecting the solitary wave (4.1)-(4.2) into system (2.10). These residuals are therefore given by explicit formulae. This technique has been used in [27]. In this paper, we do not try to give some optimal convergence result and calculating the residuals explicitly is left to future work. Let us also mention that the global (time and space) order of our scheme may be limited by the order of the splitting method used here, which is of order two as already discussed by Bonneton *et al.* in [2].

4.2. **Head on collision of counter propagating solitary waves.** A standard nonlinear test case for numerical methods is the interaction of solitary wave. In this numerical test, we study an important phenomenon in the study of nonlinear dispesive waves, the head on collision of two counter propagating waves with different amplitudes. We used solitary wave solutions with correctors of order $\mathcal{O}(\varepsilon^3)$ for the eB system established in [23] and defined in (4.1)-(4.2). We consider two solitary waves centred at $x = -50$ and $x = 50$ at $t = 0$ on a spatial domain $L = 200$, see Figure 10. The solitary wave centred at $x = -50$ travels to the right with a speed $c_{s,1} = 1.0206$ and an initial amplitude $a_1 = 0.4$ while the one centred at $x = 50$ travels to the left with a speed $c_{s,2} = 1.0102$ and an initial amplitude $a_2 = 0.2$. The

domain is discretized using 1200 cells and periodic boundary conditions are imposed. The numerical solutions are computed using model (2.10) with $\varepsilon = 0.1$ and $\alpha = 1$. The collision of the two waves starts at about $t = 43$, see Figure 10. After the interaction, each wave continue moving in its own direction and turn up to be unaffected by the collision, see Figures 11 and 12. A proper description of the distinctive nature of nonlinear interactions is illustrated when zooming at the oscillating dispersive tails of very small amplitude at $t = 70$ in Figure 13. The high precision of our numerical scheme is verified after accurately capturing this phenomenon and inducing similar observations to earlier works [3, 16, 28] where the head-on collision is carried out.

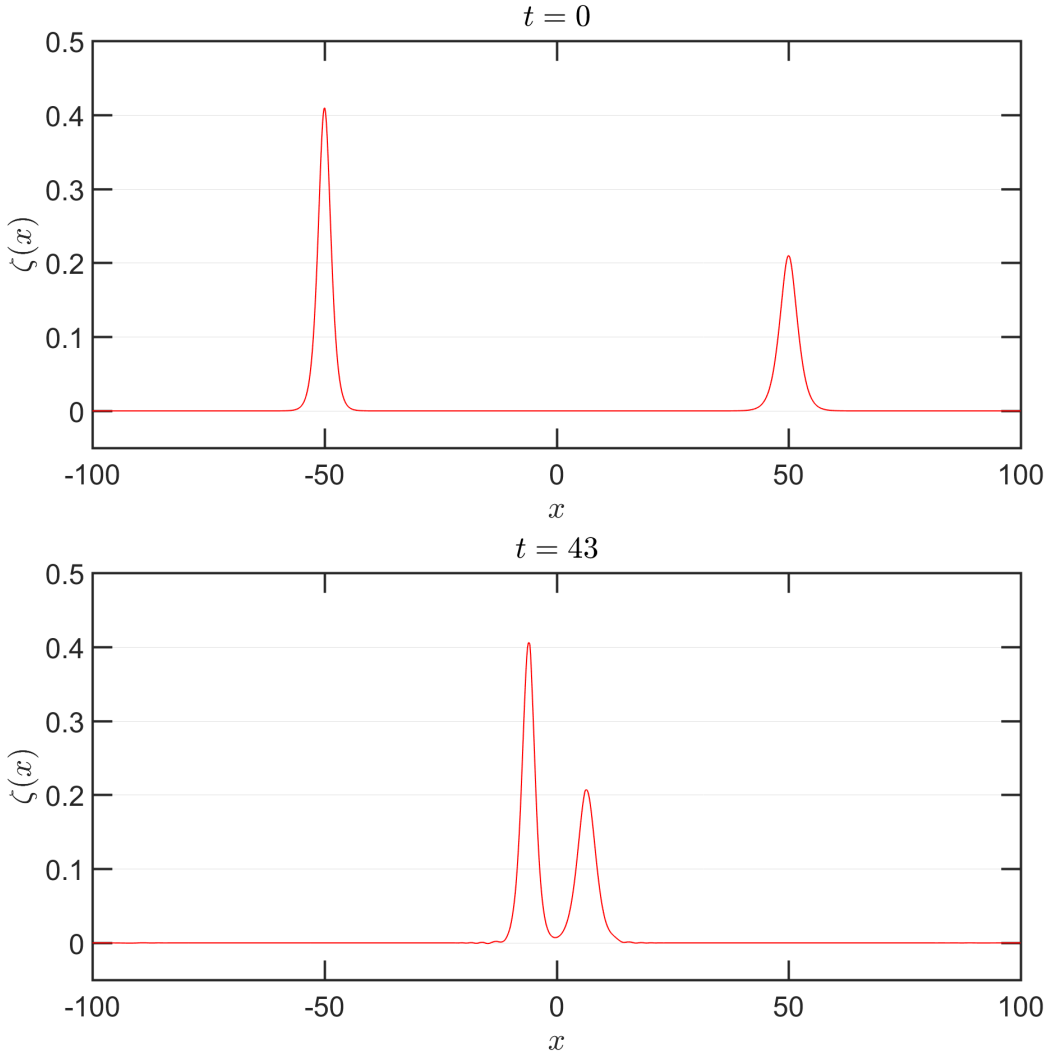

FIGURE 10. Head on collisions: surface wave shape at $t = 0$ and $t = 43$.

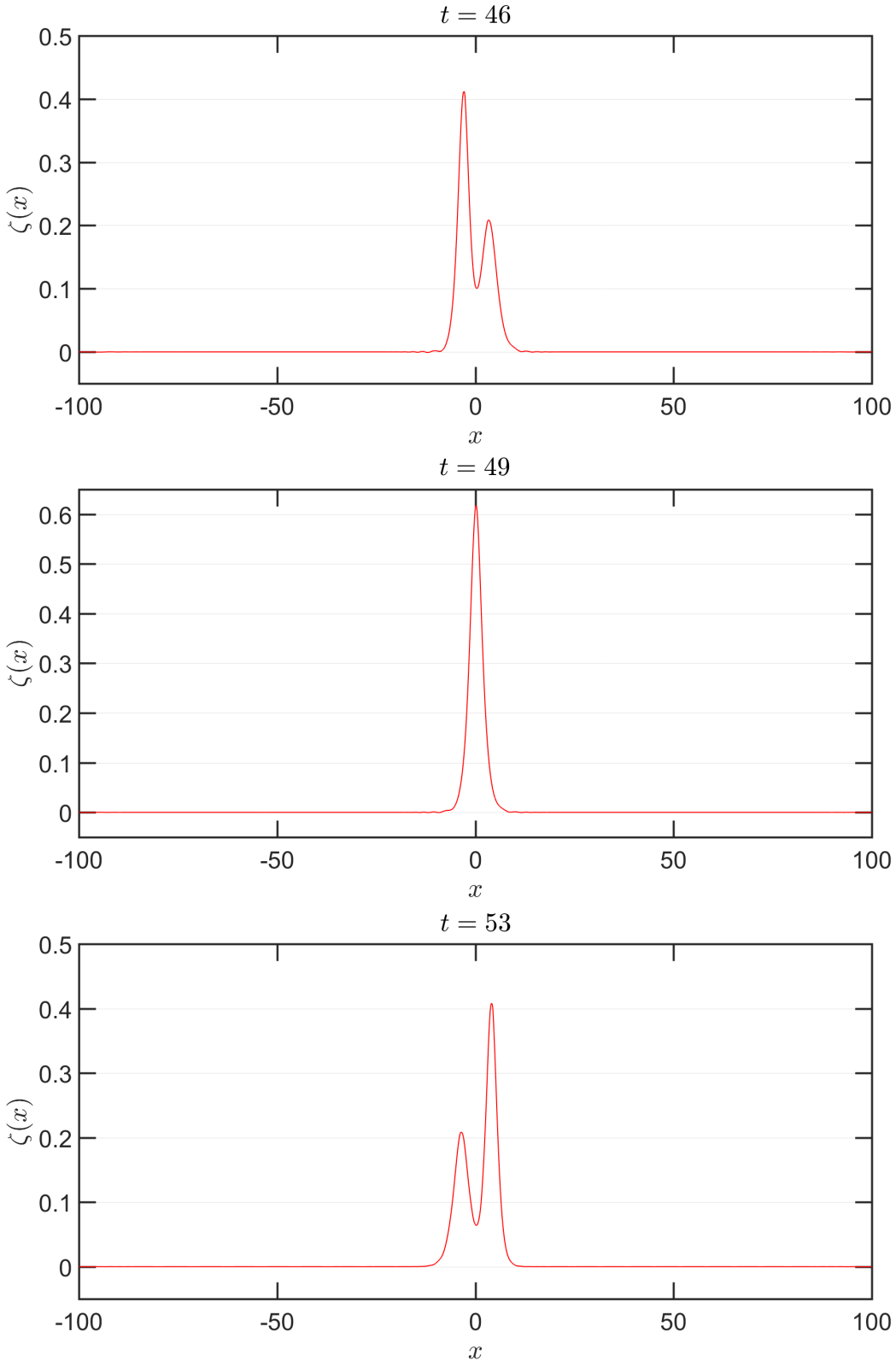

FIGURE 11. Head on collisions: surface wave shape at $t = 46, 49$ and 53.

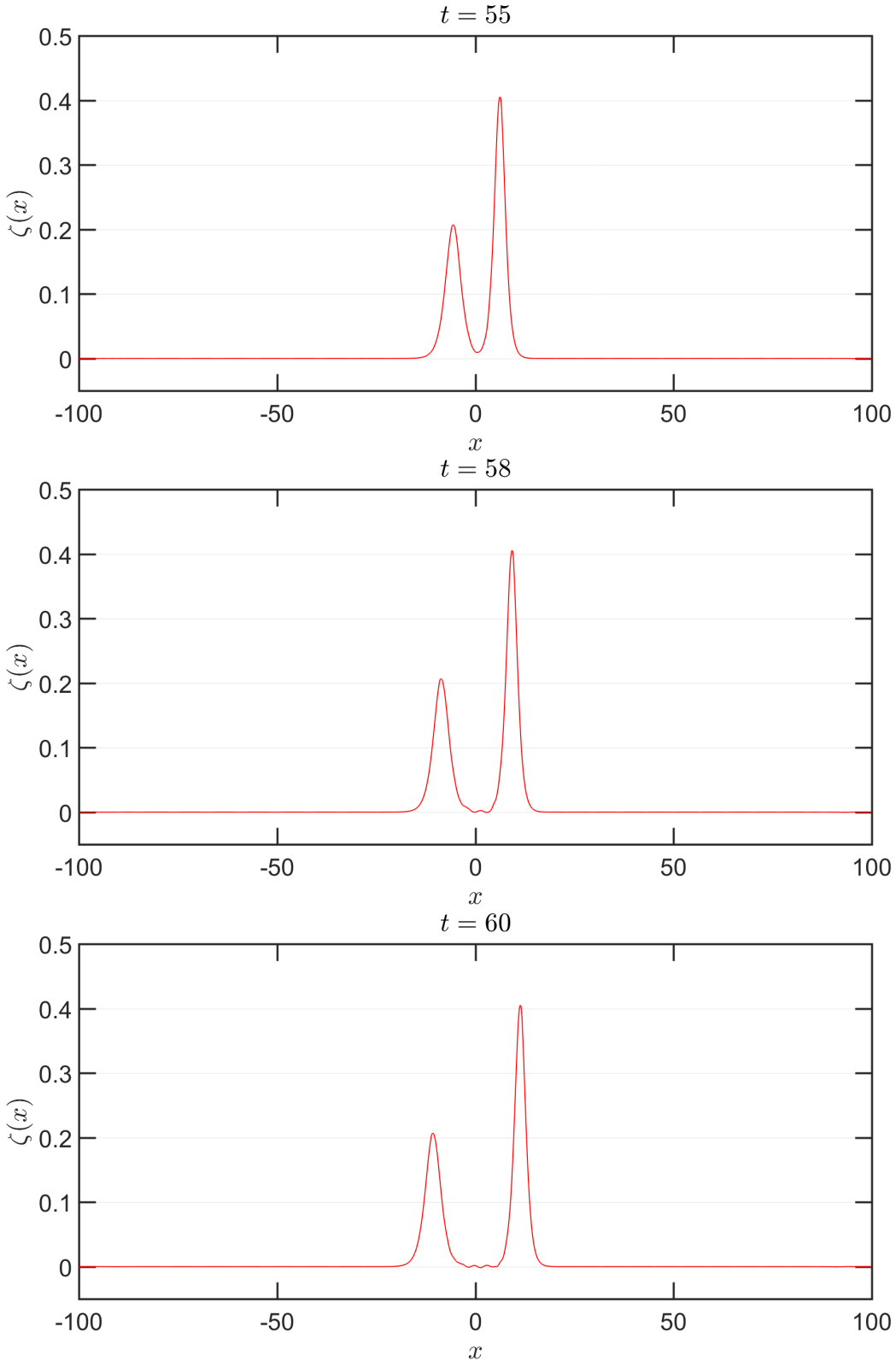

FIGURE 12. Head on collisions: surface wave shape at $t = 55, 58$ and 60.

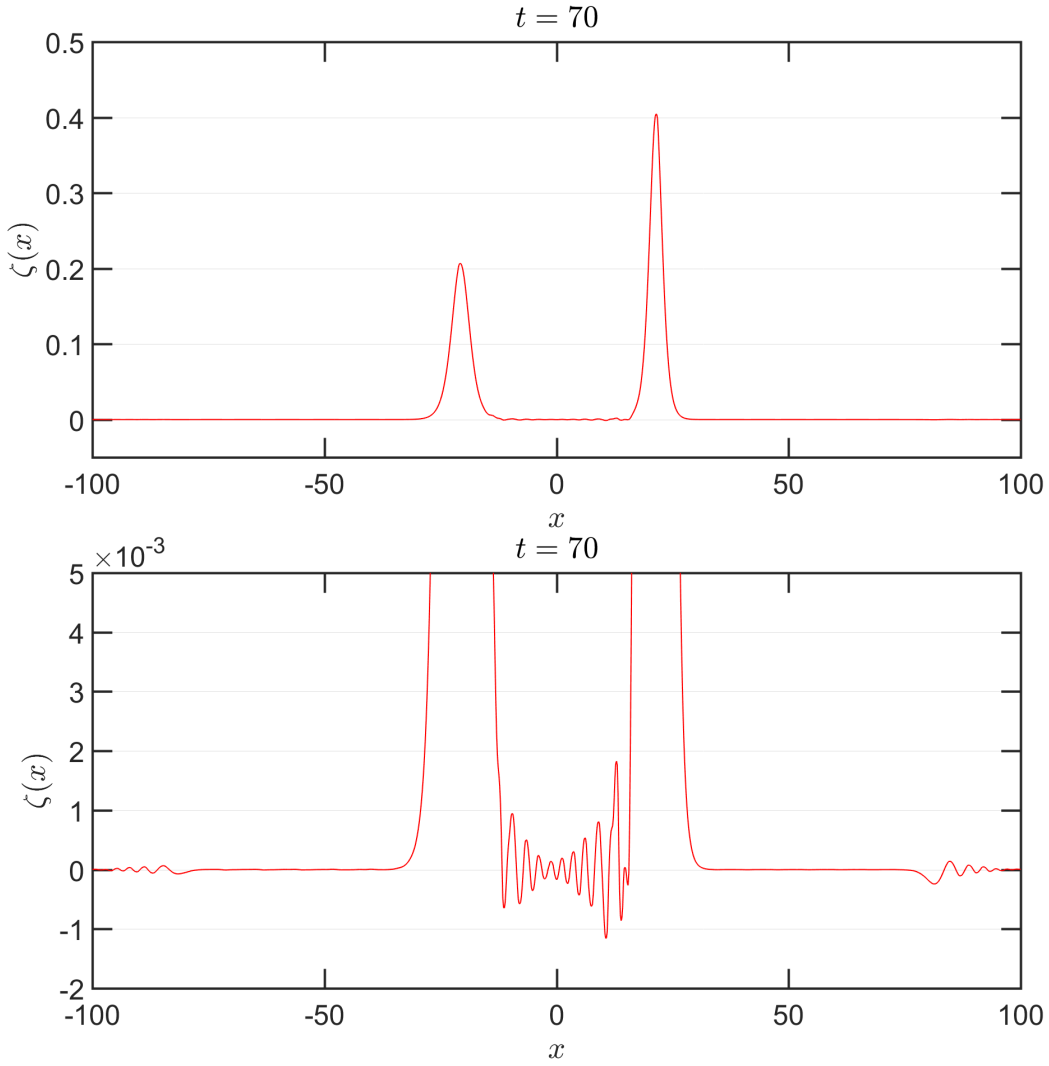

FIGURE 13. Head on collisions: surface wave shape at $t = 70$.

4.3. **Breaking of a regular heap of water with a large wave number.** In this numerical test, we highlight the importance of factorizing high order derivatives present in the improved eB model (2.10) together with an appropriate choice of the parameter α in improving the frequency dispersion in high frequency regimes. To this end, we consider a sufficiently regular heap of water with a large wavenumber represented by the initial data:

$$\zeta(0, x) = 0.7e^{-80x^2}, \ v(0, x) = 0,$$

(dashed lines) with a domain of computation $x \in (-2, 2)$ discretized with 512 cells and under periodic boundary conditions. The nonlinearity parameter is set as follow: $\varepsilon = 0.1$ (non-dimensional setting). Our numerical solutions are computed using models (2.6) and (2.10). We compare our numerical solutions with the numerical solutions computed using the Matlab script of Duchêne, Israwi and Talhouk [14] and with the GN-CH model obtained in [3]. The frequency dispersion of the original Green-Naghdi models describing a two-layer flow is improved in [14] by introducing a new class of tailored Green-Naghdi models with a slight modification of the dispersion components using a class of Fourier multipliers. One can easily recover the one-layer configuration by setting $\gamma = 0$ and $\delta = 1$. In [14], the authors compute the solution of the obtained Green-Naghdi systems by using spectral methods [43] for spatial discretization and the Matlab solver ode45 for temporal discretization. In this numerical test, we compare th numerical solutions of the proposed model eB, with the solutions corresponding to the "improved" Green-Naghi model. This model enjoys the same dispersion relation as the one of the *full Euler system*. In [3], the authors improve the frequency dispersion of the original Green–Naghdi model in

the Camassa–Holm regime (GN-CH) describing a two-layer flow thanks to a new reformulation with a suitably chosen parameter α keeping the same order of precision as the original one, namely $\mathcal{O}(\mu^2, \mu\varepsilon^2)$. One can easily recover the one-layer configuration by setting $\gamma = 0$ and $\delta = 1$. Using similar numerical methods to the one adopted in this paper, in [3] the authors solve numerically the GN-CH model.

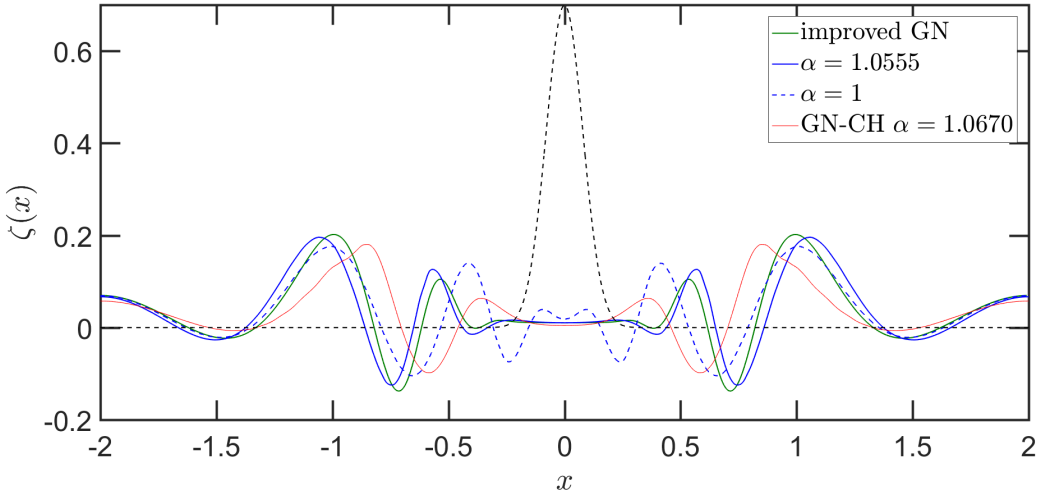

(a) Comparison of the numerical solutions of model (2.10) (blue) with the "improved" GN model (green) and the GN-CH model (red).

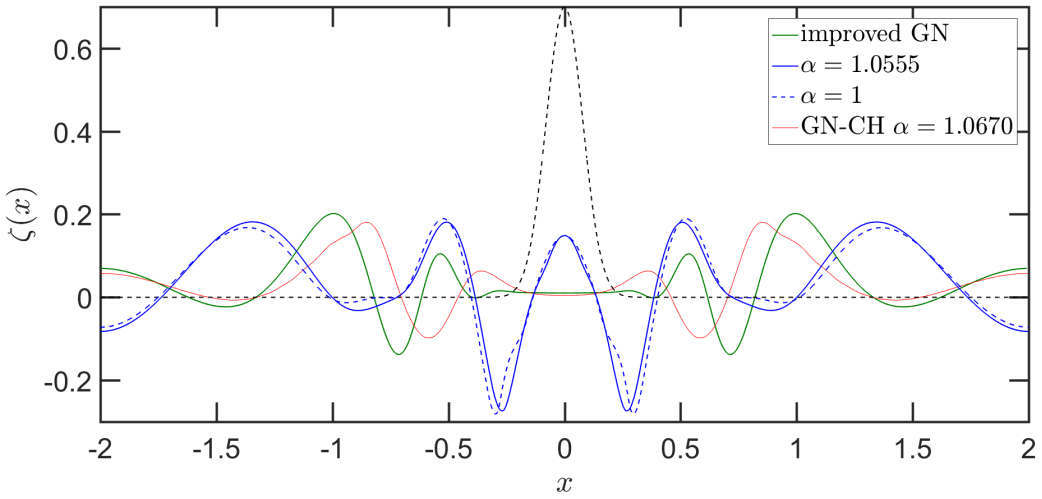

(b) Comparison of the numerical solutions of model (2.6) (blue) with the "improved" GN model (green) and the GN-CH model (red).

FIGURE 14. Comparison of the numerical solutions of model (2.10) and model (2.6) with the "improved" GN model and the GN-CH model [3] at $t = 3$.

Figure 14(a) shows when α is chosen appropriately as discussed in section 2.3, namely $\alpha_{opt} = 1.0555$, our numerical solution computed over a sufficient duration $t = 3$ using model (2.10) behave similarly to the one computed with the "improved" Green-Naghdi model. In contrary, when choosing $\alpha_{opt} = 1$ or when using the model (2.6) to compute the solution (Figure 14 (b)), the behaviour is different than the "improved" Green-Naghdi model. The GN-CH model has an improved frequency dispersion due to the careful choice of the parameter α. Nevertheless, the numerical solution computed using the GN-CH model is far from the numerical solution of the "improved" Green-Naghdi model. In fact, the eB model (2.10) is precise up to $\mathcal{O}(\varepsilon^3)$ order and thus contains high-order dispersive terms that are neglected in the GN-CH model. This explains the fair agreement in high frequency regime between the numerical

solutions of the "improved" Green-Naghdi model and the eB model (2.10) rather than the GN-CH model. One can see that the choice of an optimal value of α when using the model (2.6) has no beneficial effect due to the high frequency regime setting. This numerical test confirms that the model (2.6) has a range of applicability limited to $k \leq 1$ and thus has poor dispersion properties in intermediate and large wave numbers regime unlike model (2.10) who enjoys an extended range of applicability and a dispersion relation similar to the one of the *full Euler* system when α is appropriately chosen (see discussion in section 2.3). One can deduce the importance of using the model (2.10) containing factorized high order derivatives along with an optimal choice of α in the implementation of smooth data with high frequencies.

4.4. **Breaking of a regular heap of water with a small wave number.** In this numerical test, we consider the breaking of a sufficiently regular heap of water with a small wavenumber whose initial data is:

$$\zeta(0,x) = 0.7e^{-0.4x^2}, \ v(0,x) = 0,$$

(dashed lines) within a domain of computation $x \in (-2,2)$ discretized with 512 cells and under periodic boundary conditions. The nonlinearity parameter is set as follow: $\varepsilon = 0.5$ (non-dimensional setting). Our numerical solutions are computed using models (2.6) and (2.10) and compared with the numerical solution of the "improved" Green-Naghdi model and the numerical solution of the GN-CH model [3] over a sufficient duration $t = 3$. The parameter α is fixed as 1. In fact, both eB models (2.6) and (2.10) have an equivalent dispersion relation to the one of the *full Euler* system for small wave numbers whenever $\alpha = 1$. Indeed, Figure 15 shows a fairly good agreement between the solutions of the eB models (2.6) (yellow line) and (2.10) (blue line), and the solution of the GN-CH model [3] (red line) and the one of the "improved" Green-Naghdi model (green line). This confirms the fact that all the aforementioned models behave similarly in small wavenumbers regime, hence one can deduce that these models enjoys similar dispersive properties as the one of the *full Euler* system in small wavenumbers regime.

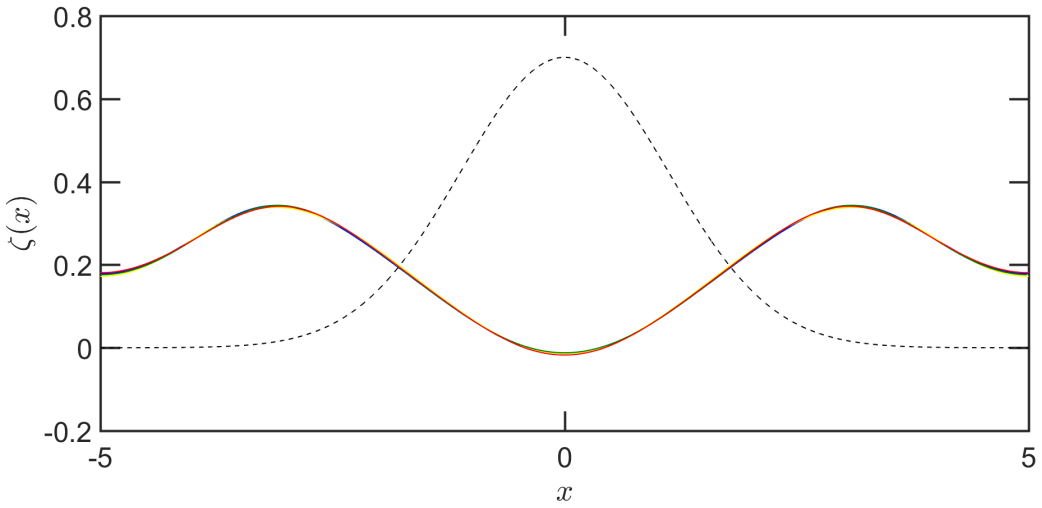

FIGURE 15. Comparison of the numerical solutions of model (2.10) (blue line) and model (2.6) (yellow line) and the GN-CH model [3] (red line) with the "improved" Green-Naghdi model (green line) at $t = 3$.

4.5. **Dam-break problem.** Dealing with non-regular solutions needs a special treatment at the numerical scheme level. Earlier works [2, 9, 27] have shown that the use of high-order schemes in dispersive waves study is necessary to prevent the corruption of the dispersive properties of the model. In general, dispersive shock waves are generated due to the dispersive effects [28, 37] when considering discontinuous initial data. In this numerical test, we implement a dam break problem in order to investigate the performance of our numerical scheme in handling non-regular solutions. We consider the following initial data:

$$\zeta(0,x) = a[1 + \tanh(250 - |x|)], \quad v(0,x) = 0, \tag{4.5}$$

with $a = 0.2091\ m$ defined on the computational domain $x \in (-700, 700)$ discretized using 2800 cells and imposed under periodic boundary conditions. The solutions are computed using the model (2.17) knowing that similar results were obtained when using the model (2.19). In this test, the choice of α is not important, thus we choose $\alpha = 1$.

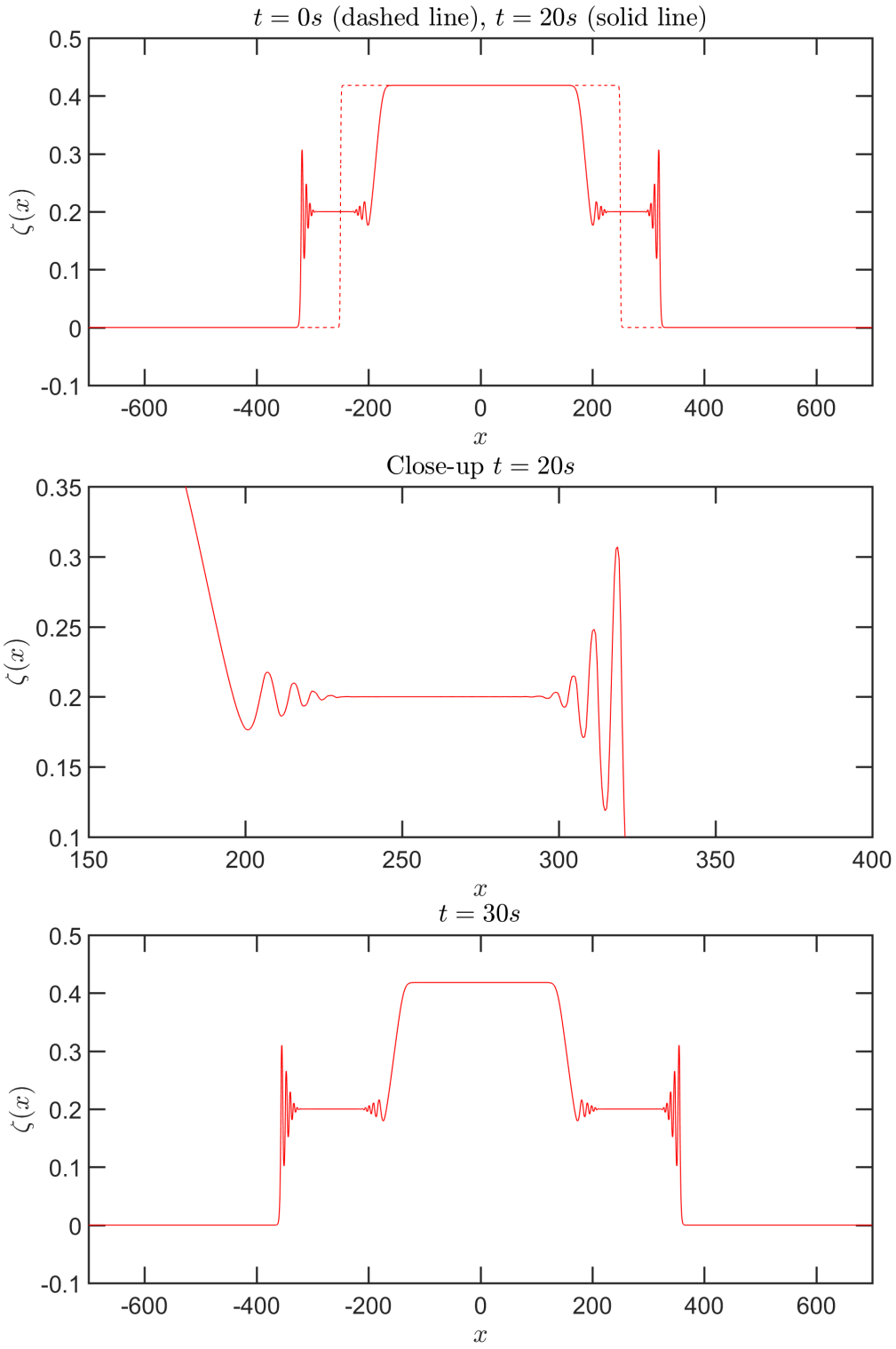

FIGURE 16. Dam break: wave shape at $t = 0s, 20s$ and $30s$.

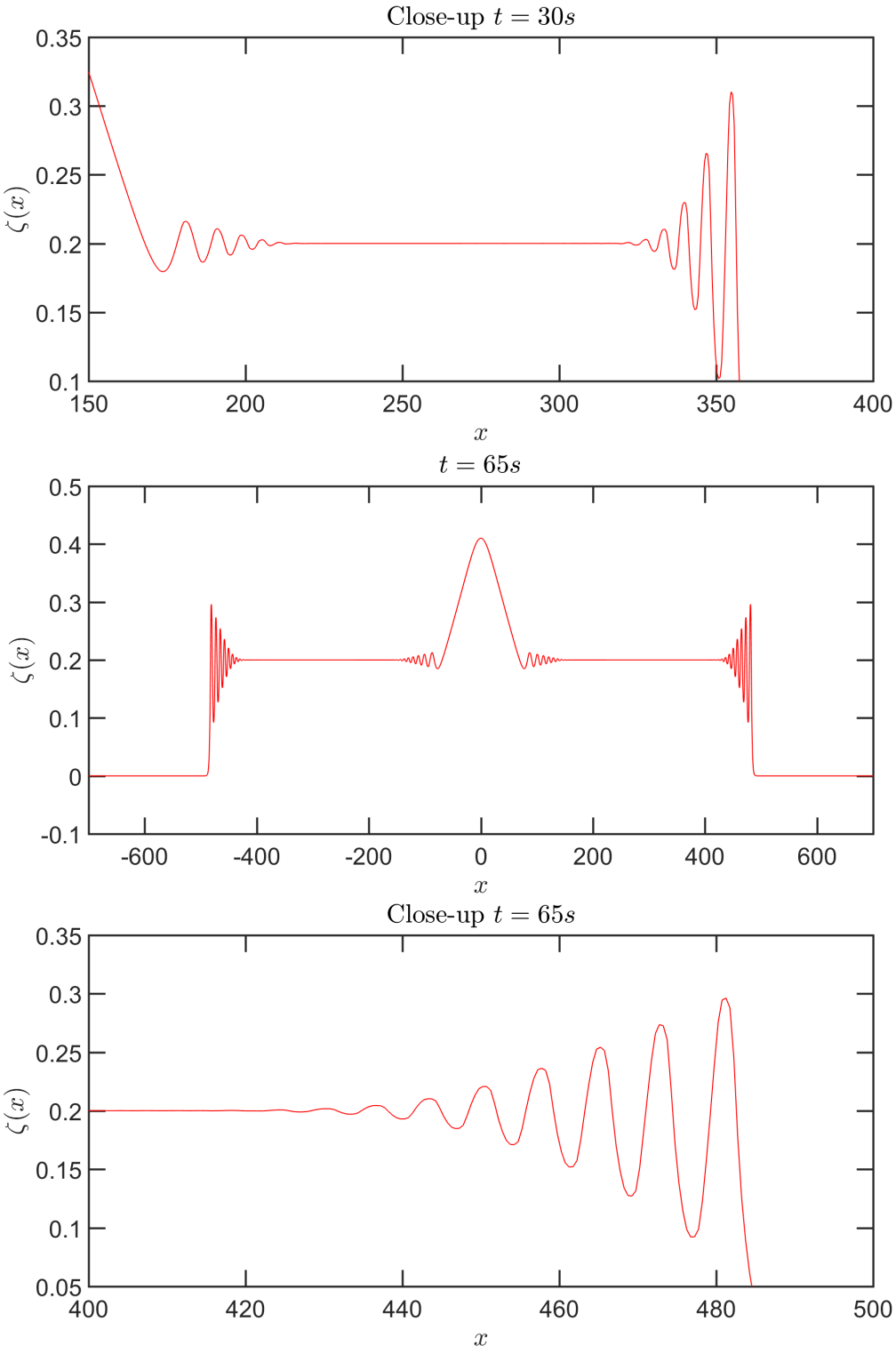

FIGURE 17. Dam break: wave shape at $t = 30s$ and $t = 65s$.

The dam break wave shape is shown at different times in Figures 16 and 17. The initial data breaks and generates dispersive shock waves. A close-up on the profiles at $t = 20s$, $t = 30s$ and $t = 65s$ shows two dispersive shock waves counter-propagating on both sides of the "dam", and two rarefaction waves moving in the direction of the center. This shows that our high-order numerical scheme was able to capture accurately this phenomenon. Dispersive shock waves in a large class of dispersive shallow

water models were carried out in several works [3, 16, 28, 37, 36] and show a good agreement with our numerical simulation.

References

[1] J. L. Bona, T. Colin, and D. Lannes, *Long wave approximations for water waves*, Arch. Ration. Mech. Anal., 178 (2005), pp. 373–410.

[2] P. Bonneton, F. Chazel, D. Lannes, F. Marche, and M. Tissier, *A splitting approach for the fully nonlinear and weakly dispersive Green-Naghdi model*, J. Comput. Phys., 230 (2011), pp. 1479–1498.

[3] C. Bourdarias, S. Gerbi, and R. Lteif, *A numerical scheme for an improved Green-Naghdi model in the Camassa-Holm regime for the propagation of internal waves*, Comput. & Fluids, 156 (2017), pp. 283–304.

[4] ———, *A numerical scheme for the propagation of internal waves in an oceanographic model*, in Finite volumes for complex applications VIII—hyperbolic, elliptic and parabolic problems, vol. 200 of Springer Proc. Math. Stat., Springer, Cham, 2017, pp. 101–108.

[5] J. Boussinesq, *Théorie de l'intumescence liquide appelée onde solitaire ou de translation se propageant dans un canal rectangulaire*, C.R. Acad. Sci. Paris Sér. A-B, 72 (1871), pp. 755–759.

[6] J. Boussinesq, *Théorie des ondes et des remous qui se propagent le long d'un canal rectangulaire horizontal, en communiquant au liquide contenu dans ce canal des vitesses sensiblement pareilles de la surface au fond.*, J. Math. Pures Appl., 17 (1872), pp. 55–108.

[7] C. Burtea, *New long time existence results for a class of Boussinesq-type systems*, Journal de Mathématiques Pures et Appliquées, 106 (2016), pp. 203 – 236.

[8] F. Chazel, *Influence of bottom topography on long water waves*, M2AN Math. Model. Numer. Anal., 41 (2007), pp. 771–799.

[9] F. Chazel, D. Lannes, and F. Marche, *Numerical simulation of strongly nonlinear and dispersive waves using a Green-Naghdi model*, J. Sci. Comput., 48 (2011), pp. 105–116.

[10] R. Cienfuegos, E. Barthélemy, and P. Bonneton, *A fourth-order compact finite volume scheme for fully nonlinear and weakly dispersive Boussinesq-type equations. II. Boundary conditions and validation*, Internat. J. Numer. Methods Fluids, 53 (2007), pp. 1423–1455.

[11] W. Craig and C. Sulem, *Numerical simulation of gravity waves*, J. Comput. Phys., 108 (1993), pp. 73–83.

[12] W. Craig, C. Sulem, and P.-L. Sulem, *Nonlinear modulation of gravity waves: a rigorous approach*, Nonlinearity, 5 (1992), pp. 497–522.

[13] V. Duchêne, S. Israwi, and R. Talhouk, *Shallow water asymptotic models for the propagation of internal waves*, Discrete Contin. Dyn. Syst. Ser. S, 7 (2014), pp. 239–269.

[14] V. Duchêne, S. Israwi, and R. Talhouk, *A new class of two-layer Green-Naghdi systems with improved frequency dispersion*, Stud. Appl. Math., 137 (2016), pp. 356–415.

[15] A. Duran and F. Marche, *Discontinuous-Galerkin discretization of a new class of Green-Naghdi equations*, Commun. Comput. Phys., 17 (2015), pp. 721–760.

[16] G. A. El, R. H. J. Grimshaw, and N. F. Smyth, *Unsteady undular bores in fully nonlinear shallow-water theory*, Phys. Fluids, 18 (2006), pp. 027104, 17.

[17] K. S. Erduran, S. Ilic, and V. Kutija, *Hybrid finite-volume finite-difference scheme for the solution of Boussinesq equations*, Internat. J. Numer. Methods Fluids, 49 (2005), pp. 1213–1232.

[18] S. S. Frazao and Y. Zech, *Undular bores and secondary waves -experiments and hybrid finite-volume modelling*, Journal of Hydraulic Research, 40 (2002), pp. 33–43.

[19] M. F. Gobbi, J. T. Kirby, and G. Wei, *A fully nonlinear Boussinesq model for surface waves. II. Extension to $O(kh)^4$*, J. Fluid Mech., 405 (2000), pp. 181–210.

[20] A. E. Green and P. M. Naghdi, *A derivation of equations for wave propagation in water of variable depth*, J. Fluid Mech., 78 (1976), pp. 237–246.

[21] G.-S. Jiang and C.-W. Shu, *Efficient implementation of weighted ENO schemes*, J. Comput. Phys., 126 (1996), pp. 202–228.

[22] B. Khorbatly and S. Israwi, *Full justification for the extended Green-Naghdi system for an uneven bottom with surface tension*. Preprint, hal-02994586, (2020).

[23] B. Khorbatly, R. Lteif, S. Israwi, and S. Gerbi, *Mathematical modeling and numerical analysis for the higher order Boussinesq system*, Preprint, arXiv:2102.08045, (2021).

[24] B. Khorbatly, I. Zaiter, and S. Israwi, *Derivation and well-posedness of the extended Green-Naghdi equations for flat bottoms with surface tension*, Journal of Mathematical Physics, 59 (2018), p. 071501.

[25] J. Kirby, *Nonlinear, dispersive long waves in water of variable depth*, Advances in Fluid Mechanics, 10 (1996), p. 75.

[26] D. Lannes, *The water waves problem*, vol. 188 of Mathematical Surveys and Monographs, American Mathematical Society, Providence, RI, 2013. Mathematical analysis and asymptotics.

[27] D. Lannes and F. Marche, *A new class of fully nonlinear and weakly dispersive Green-Naghdi models for efficient 2D simulations*, J. Comput. Phys., 282 (2015), pp. 238–268.

[28] O. Le Métayer, S. Gavrilyuk, and S. Hank, *A numerical scheme for the Green-Naghdi model*, J. Comput. Phys., 229 (2010), pp. 2034–2045.

[29] F. Linares, D. Pilod, and J. Saut, *Well-posedness of strongly dispersive two-dimensional surface wave Boussinesq systems*, SIAM J. Math. Anal., 44 (2012), pp. 4195–4221.

[30] P. A. Madsen, H. B. Bingham, and H. A. Schäffer, *Boussinesq-type formulations for fully nonlinear and extremely dispersive water waves: derivation and analysis*, Proceedings of the Royal Society of London. Series A: Mathematical, Physical and Engineering Sciences, 459 (2003), pp. 1075–1104.

[31] P. A. Madsen, R. Murray, and O. R. Sørensen, *A new form of the Boussinesq equations with improved linear dispersion characteristics*, Coastal Engineering, 15 (1991), pp. 371 – 388.
[32] P. A. Madsen and H. A. Schäffer, *Higher-order Boussinesq-type equations for surface gravity waves: derivation and analysis*, R. Soc. Lond. Philos. Trans. Ser. A Math. Phys. Eng. Sci., 356 (1998), pp. 3123–3184.
[33] Y. Matsuno, *Hamiltonian formulation of the extended Green–Naghdi equations*, Physica D: Nonlinear Phenomena, 301-302 (2015), pp. 1 – 7.
[34] ———, *Hamiltonian structure for two-dimensional extended Green–Naghdi equations*, Proc. R. Soc. A., 472 (2016).
[35] M. Ming, J. C. Saut, and P. Zhang, *Long-time existence of solutions to Boussinesq systems*, SIAM J. Math. Anal., 44 (2012), pp. 4078–4100.
[36] D. Mitsotakis, D. Dutykh, and J. Carter, *On the nonlinear dynamics of the traveling-wave solutions of the serre system*, Wave Motion, 70 (2017), pp. 166 – 182. Recent Advances on Wave Motion in Fluids and Solids.
[37] D. Mitsotakis, B. Ilan, and D. Dutykh, *On the Galerkin/finite-element method for the Serre equations*, J. Sci. Comput., 61 (2014), pp. 166–195.
[38] J. Saut, C. C. Wang, and L. Xu, *The cauchy problem on large time for surface-waves-type Boussinesq systems ii*, SIAM J. Math. Anal., 49 (2017), pp. 2321–2386.
[39] J.-C. Saut and L. Xu, *The Cauchy problem on large time for surface waves Boussinesq systems*, J. Math. Pures Appl. (9), 97 (2012), pp. 635–662.
[40] C.-W. Shu, *Essentially non-oscillatory and weighted essentially non-oscillatory schemes for hyperbolic conservation laws*, in Advanced numerical approximation of nonlinear hyperbolic equations (Cetraro, 1997), vol. 1697 of Lecture Notes in Math., Springer, Berlin, 1998, pp. 325–432.
[41] J. Stoker, *Water Waves: The mathematical theory with applications*, Interscience, New York, (1957).
[42] M. Tissier, P. Bonneton, F. Marche, F. Chazel, and D. Lannes, *A new approach to handle wave breaking in fully non-linear Boussinesq models*, Coastal Engineering, 67 (2012), pp. 54 – 66.
[43] L. N. Trefethen, *Spectral methods in MATLAB*, vol. 10 of Software, Environments, and Tools, Society for Industrial and Applied Mathematics (SIAM), Philadelphia, PA, 2000.
[44] J. M. Witting, *A unified model for the evolution nonlinear water waves*, Journal of Computational Physics, 56 (1984), pp. 203 – 236.
[45] V. E. Zakharov, *Stability of periodic waves of finite amplitude on the surface of a deep fluid*, Journal of Applied Mechanics and Technical Physics, 9 (1968), pp. 190–194.

Laboratoire de Mathématiques UMR 5127 CNRS & Université de Savoie Mont Blanc, Campus scientifique, 73376 Le Bourget du Lac Cedex, France
Email address: stephane.gerbi@univ-smb.fr

Lebanese American University (LAU), Graduate Studies and Research (GSR) office, School of Arts and Sciences, Computer Science and Mathematics Department, Beirut, Lebanon
Email address: Corresponding author, ralph.lteif@lau.edu.lb